V. Muscarello, G. Quaranta
Structural Coupling and Whirl-Flutter Stability with Pilot-In-the-loop
Journal of the American Helicopter Society, In press - Published online 10/03/2021
doi:10.4050/JAHS.66.032003

Structural Coupling and Whirl-Flutter Stability with Pilot-in-the-loop

Vincenzo Muscarello*, Giuseppe Quaranta

Dept. of Aerospace Science and Technology, Politecnico di Milano,

Milano, Italy, 20156

Abstract

This paper investigates structural coupling problems for tiltrotors, considering not only the interaction of the flight control system with the flexible structure, but also the potentially adverse effects on the aeroservoelastic stability that may be caused by the pilot's involuntary, high-frequency, biodynamic response. The investigation is focused on the analysis of the side effects that could appear at high speed in the airplane flight regime, where the whirl flutter boundaries may be significantly reduced. A detailed tiltrotor model, representative of the Bell XV-15 and of a flight control system has been built and joined with a pilot biodynamic model acting on the power-lever and on the center stick, available in the literature. Additionally, a modified version of the XV-15 using differential collective pitch for yaw control in airplane mode instead of rudder has been investigated, to show the effect of different yaw control designs.

The stability analyses presented demonstrate that the structural coupling analysis and the flutter boundaries for tiltrotors must be evaluated not only considering the closed loop created by the flight control system, but also the effect of involuntary pilot response. Sensitivity analyses examine the most critical parameters impacting tiltrotor aeroservoelastic stability. Finally, the employment of notch filters as a means of prevention is discussed.

*Corresponding author (vincenzo.muscarello@polimi.it).

Nomenclature

$\mathbf{A}_a, \mathbf{B}_a, \mathbf{C}_a, \mathbf{D}_{a_0}, \mathbf{D}_{a_1}, \mathbf{D}_{a_2}$	airframe unsteady aerodynamics state space matrices
$a_X^{seat}, a_Y^{seat}, a_Z^{seat}$	longitudinal, lateral and vertical accelerations measured at the pilot's seat
$\mathbf{f}_a$	vector of generalized unsteady aerodynamic forces
G_p	pilot biomechanical static gain
$H_c(s), H_m(s)$	servo-valve and dynamic compliance transfer functions
I_E	engine reduced inertia
K_{1P}, K_{1R}, K_{1Y}	pitch, roll and yaw overshoot ratios in control shaping transfer functions
K_{2P}, K_{2R}	pitch and roll axis disturbance rejection mode lagged rate feedback gains
K_{2Y}	yaw axis disturbance rejection mode rate feedback gain
K_{3P}, K_{3R}	pitch and roll axis rate feedback gains
K_{4P}, K_{4R}	design pitch rate and roll rate steady state response
K_{5P}, K_{5R}	pitch and roll axis attitude feedback gains
K_{7P}, K_{7R}	pitch and roll axis disturbance rejection mode rate feedback gains
K_E, K_I, K_M	engine, inter-connect and rotor shaft reduced stiffnesses
k	reduced frequency
M_∞	Mach number
m_c	control surface reaction moment
P	rotor power
Q	notch filter quality factor
$\mathbf{Q}_{hh}(k, M_\infty)$	aerodynamic transfer matrix associated with the structural mode shapes
$\mathbf{Q}_{hg}(k, M_\infty)$	aerodynamic transfer matrix associated with the gust input
$\mathbf{q}$	vector of generalized coordinates
q_∞	dynamic pressure
r_E	gear ratio between engine rotational speed and rotor speed
r_I	gear ratio between inter-connect shaft rotational speed and rotor speed
s	Laplace's variable

T	rotor thrust
T_p	pilot biomechanical time delay
T_{1P}, T_{1R}, T_{1Y}	design pitch, roll and yaw rate time constants
T_{2P}, T_{2R}, T_{2Y}	pitch, roll and yaw washout time constants in disturbance rejection loop
V_∞	airstream velocity
$\mathbf{v}_g$	vector of gust velocities
X_{COL}	vertical power-lever position
X_{LN}, X_{LT}	longitudinal and lateral center stick position
X_{PD}	pedals position
$\mathbf{x}_a$	airframe aerodynamics state space vector
$\beta_0, \beta_{1C}, \beta_{1S}$	rotor coning, longitudinal and lateral flapping angles
δ_E	elevator angle
ζ	damping ratio
θ	pitch attitude angle
ϑ	control surface deflection
ϑ_c	requested control surface deflection/pilot's demand
$\vartheta_0, \vartheta_{1S}$	rotor collective and longitudinal cyclic pitch angles
μ	slope in gain at the notch frequency
μ_∞	notch filter nondimensional gain value for infinite frequency
τ	climb angle
Ω	rotor speed
ω_n	natural frequency
ω_{NF}	notch filter frequency
$(\cdot)^T$	variable at trim condition

Introduction

The Flight Control System (FCS) is an essential part of modern rotorcraft. The expected enhancement of handling qualities and the reduction of pilot workload, with the promise of greater safety, are increasing the number of fixed and rotary-wing aircraft designs equipped with FCS (Ref. 1). In tiltrotors, the inclusion of digital fly-by-wire FCS is becoming the preferred option, since it also provides the control mixing as a function of the flight speed and nacelle angle to permit a smooth transition between helicopter and airplane flight regimes.

The FCS establishes a feedback loop between the measurements coming from inertial sensors and the aircraft controls. The FCS is usually designed to control the rigid-body motion. However, the inertial sensors are fitted into the deformable airframe, and thus they pick up structural vibrations as well, unless appropriate filtering is used. This spill-over may cause problems when the FCS responds to aeroservoelastic excitation (Ref. 2). The investigation of the possible coupling between the dynamic response of the airframe and the FCS is known as Structural Coupling (SC), and plays a very important role in the qualification of aircraft with digital controls.

A historical perspective of SC problems encountered in the fixed-wing community is reported by Caldwell in Ref. 3. Development of analysis tools and procedures to address the problem, as experienced in aircraft flight control design at Warton, began in the early 1960s with the TSR-2 aircraft, and have continued to present. In recent times, SC problems on rotary-wing aircraft have received considerable attention. The ground resonance phenomenon, augmented by the FCS, was investigated by Masarati et al. in Ref. 4. SC problems have been also identified in tiltrotor development. During the XV-15 flight test program, damping in one of the antisymmetric wing modes was less than predicted when the stability and control augmentation system (SCAS) was turned on (Ref. 5). Similar events occurred on the Bell Boeing V-22 Osprey and Bell Agusta BA609 (now Leonardo Helicopters AW609, Ref. 5, 6). It can be expected that the development of new civil tiltrotors, characterized by lighter structures, may increase SC problems that must be carefully investigated during the design phase.

To investigate the problem on a realistic case, it has been decided to focus the analysis on the XV-15, since a large amount of data are publicly available. A detailed model, representative of the Bell XV-15

with advanced technology blades (ATBs, Ref. 7), has been assembled. The three-bladed rotors consist of a gimbal, represented by a universal joint, a stiff-in-plane hub and no lateral cyclic controls. The airframe model has been modified with a thinner wing (15% t/c), later denoted as "thin-wing", to reduce the elastic natural frequencies, increasing SC sensitivity. A linearized FCS, with scheduled control laws that are functions of the flight condition, has been introduced to analyze the overall stability on the extended frequency band, ranging from the flight mechanics up to structural modes.

With respect to classical elements of SC analysis reported by Caldwell (Ref. 3), for a rotorcraft it is important to consider the additional feedback generated by the pilot, which could in some cases cause unstable rotorcraft-pilot couplings. These phenomena occur when feedback loops created in the pilot-vehicle system become unstable, leading to a divergent uncontrolled motion (Ref. 8).

Classical rotorcraft-pilot coupling events caused by the pilot's erroneous perception of the vehicle dynamics lead to pilot induced oscillations (PIOs), where the main cause is a voluntary, out-of-phase, control input introduced by the pilot (Ref. 9). However, there is a second feedback loop caused by the vibrations that are injected in the cockpit and transmitted through pilot's body into the inceptors. In this case, the feedback loop is dominated by the involuntary biodynamic action exerted by the pilot, and the related phenomena are usually indicated in the literature as pilot assisted oscillations (PAO), to highlight the transmission role of the pilot, see Fig. 1. Usually PAOs happen in the frequency range between 2–8 Hz (Ref. 10). In PAOs the airframe vibrations are transferred through the biodynamic feedthrough (BDFT) into control input that in turn cause new structural vibrations. While PAO phenomena have also been identified in fixed-wing aircraft, it is on rotorcraft that they showed a very high incidence (Ref. 8). Rotorcraft are more susceptible to those high-frequency occurrences since their high-order dynamics play a prominent role. The control inputs given by pilots, through the cockpit inceptors, are transmitted through the swashplate to the blades, thus affecting rotor flapping and control moments transferred to the airframe. The rotating mechanism is able to generate for any control at frequency ω, oscillations at $\omega \pm \Omega$, where Ω is the angular speed of the rotor. Thus, low-frequency pilot inputs generate high-frequency blade excitation (Ref. 8). An interesting analysis of the effects of pilot's BDFT on the V-22 was presented in Ref. 6. A more complete analysis of all PAO phenomena that can happen on a tiltrotor, without considering the interaction with the FCS, can be found in Ref. 11.

The aim of the present paper is to show how the FCS is indeed able to improve the handling qualities, and to reduce the pilot workload, acting on the low frequency flight mechanics roots, although the aeroservoelastic stability could be significantly degraded. In addition, the combination with the second feedback loop due to involuntary pilot's response, may lead to significant reduction of the flutter-free flight envelope, if due care is not taken.

The paper proceeds as follows: the first section is dedicated to the introduction to tiltrotor aeroservoelastic stability problems. The next section is dedicated to the description of the tiltrotor dynamic model. The subsystems that are part of the model (airframe structure, unsteady aerodynamics, aeroelastic rotors, servo-actuators, FCS and pilot's biodynamics) are outlined. Then, the overall stability analysis including FCS and pilot's BDFT is carried out and results are discussed. A Sensitivity analysis is added, considering the effect of wing thickness and the most critical FCS and pilot's BDFT parameters for aeroservoelastic stability. Finally, possible means of prevention to mitigate SC problems are taken into account. The last section ends by drawing some conclusions.

Tiltrotor Aeroservoelastic Stability in High-Speed Flight

To ensure that stability requirements are met on tiltrotor aircraft, the airframe structure is designed to avoid whirl flutter phenomena all over the flight envelope. The whirl flutter is an aeroelastic instability that affects tiltrotors during high speed flights. This phenomenon may occur in flexible mounted wing-propeller systems, and requires one to take into account the influence of rotating masses producing centrifugal, Coriolis, and gyroscopic forces/moments in addition to aerodynamic loads. The instability is a whirl divergence that is the result of precession-generated aerodynamic hub forces. The precession is caused by in-plane aerodynamic forces that can destabilize the pitch or yaw degree of freedom of the wing-pylon elastic suspension of the proprotor. The rotor flapping due to the gimbal mechanism, can create additional destabilizing aerodynamic forces that make the phenomenon difficult to analyze without sophisticated numerical models. Moreover, the flexible rotor modes, including the low frequency blade bending and torsional modes, lie in the whirl flutter frequency range and must be taken into account for proprotor stability. The basic phenomenon is described by Wilmer H. Reed III in Ref. 12.

This instability is a significant design driver for tiltrotors. Generally, the wing torsional stiffness requirements dictate a large thickness for the wing relative to comparable turboprop aircraft (e.g. $t/c = 23\%$ for the XV-15, V-22 and AW609). Thicker wings facilitate a larger beam-bending and torsional stiffness without penalties in terms of wing weight. The large torsional stiffness helps to reduce the pylon pitch motion thereby increasing whirl flutter stability. However, a thick wing design increases aerodynamic drag, limiting the cruise efficiency and maximum speed of the aircraft.

For the work presented here, aeroelastic stability analyses are first performed on the basic aircraft without including the FCS. The wing stiffnesses, pylon support and rotor properties are modified until the stability requirements are satisfied. Subsequently, a linearized model for the FCS is added to verify that it does not compromise the stability of the system. Biomechanical models of the pilot, acting on the power-lever and on the center stick, are also included in the feedback loop. It is worth noting that when including the FCS it is appropriate to replace "aeroelasticity" with "aeroservoelasticity" in order to account for the new forces created by the control system that are added to the classic three forces of aeroelasticity: aerodynamic, inertia and elastic. Also the pilot's BDFT can be considered as an additional control block, so its addition still falls in the field of aeroservoelasticity. SC problems may arise as a consequence of the FCS and pilot's BDFT acting separately or together with the elastic modes on the aircraft, since they operate in the same frequency band up to 10 Hz.

To anticipate as many SC problems as possible, a modular and multidisciplinary approach is recommended. It is important to have a simple tool that allows for aeroservoelastic analysis during the preliminary rotorcraft design phase, considering different levels of detail for the basic aircraft, the FCS and the pilot's BDFT. For these reasons, Politecnico di Milano developed a simulation tool called MASST (Modern Aeroservoelastic State Space Tools – Refs. 4, 13). The tool can perform massive analyses of relatively simple, yet complete modular models of complex linearized aeroservoelastic systems. Since a time domain formulation in state-space is at the core of modern control theory, the equations of motion are cast as first order time differential equations. Once this is accomplished, it is no longer necessary to use the specialized formulations usually adopted in aeroservoelastic analysis; general state-space approaches can be used instead to analyze aeroservoelastic system stability, capture SC problems and fix them by introducing appropriate notch filters on the critical feedback paths.

In the following section, the aeroservoelastic model of the XV-15 in MASST is described, including the linearized FCS and the pilot's BDFT models used for the overall stability analyses.

Multidisciplinary Model

The XV-15 aeroservoelastic model has been assembled in MASST. The dynamic model set-up includes: 1) the airframe structural model, 2) airframe unsteady aerodynamics, 3) aeroelastic rotors, 4) a lumped parameter engine drive-train model, 5) servo-actuators, 6) a linearized model of the FCS and 7) pilot/control device biomechanical models. Each component is modeled in its most natural and appropriate numerical environment and then cast into first order state-space formulation. Substructures are then connected using Craig-Bampton's component mode synthesis approach (Ref. 14). The XV-15 general characteristics are summarized in Table 1.

Basic Aircraft Model

The layout of the Bell XV-15 is similar to a turboprop aircraft. Large proprotors, coupled with turboshaft engines, are mounted on the wingtip nacelles. The rotor axis rotates from the vertical direction, for hover and helicopter mode flight, to the horizontal direction for airplane mode flight (APMODE). According to available literature (Ref. 15), the airframe structure can be modeled as a finite element (FE) stick model consisting of an elastic wing, a rigid fuselage and rigid wing-mounted nacelles. The rotors are represented by two lumped masses. The resulting model is depicted in Fig. 2(a). The stick model structural properties are revised to represent an XV-15 tiltrotor with a 15% t/c composite wing, to better reveal the aeroservoelastic stability effects and SC problems. The model is designed to capture the fundamental six lowest normal modes of the wing, i.e. symmetric/antisymmetric wing bending (SWB/AWB), symmetric/antisymmetric wing chord (SWC/AWC), and symmetric/antisymmetric wing torsion (SWT/AWT). The natural frequencies in APMODE, obtained in NASTRAN, are reported in Table 2 and compared with the original thick-wing model. All the natural frequencies are reduced as expected, although the order is preserved. Control surfaces are modeled as well. The XV-15 is supplied with seven aerodynamic control surfaces, namely two flaps, two flaperons, an elevator and two rudders.

Unsteady generalized aerodynamic forces associated with small motion of the airframe and gusts can be obtained as solutions of integro-differential equations related to harmonic boundary domain oscillation, namely the generalized aerodynamic forces frequency responses $\mathbf{f}_a$,

$$\mathbf{f}_a = q_\infty \mathbf{Q}_{hh}(k, M_\infty)\mathbf{q} + q_\infty \mathbf{Q}_{hg}(k, M_\infty)\frac{\mathbf{v}_g}{V_\infty}, \tag{1}$$

where q_∞ is the dynamic pressure, $k = \omega\ell/V_\infty$ is the reduced frequency, M_∞ is the Mach number, $\mathbf{Q}_{hh}$ and $\mathbf{Q}_{hg}$ are the aerodynamic transfer matrices associated with the structural mode shapes $\mathbf{q}$ and the gust input $\mathbf{v}_g$. Matrices $\mathbf{Q}_{hh}$ and $\mathbf{Q}_{hg}$ have been obtained using the classical Doublet Lattice Method (DLM) implemented in NASTRAN (Ref. 16). Fig. 2(b) shows the aerodynamic panels defined for the XV-15, starting from the tiltrotor aircraft geometry presented in Ref. 15. MASST casts the resulting frequency domain matrices in state-space form

$$\dot{\mathbf{x}}_a = \mathbf{A}_a\mathbf{x}_a + \mathbf{B}_a\mathbf{a} \tag{2a}$$

$$\frac{\mathbf{f}_a}{q_\infty} = \mathbf{C}_a\mathbf{x}_a + \mathbf{D}_{a_0}\mathbf{a} + \frac{\ell}{V_\infty}\mathbf{D}_{a_1}\dot{\mathbf{a}} + \left(\frac{\ell}{V_\infty}\right)^2 \mathbf{D}_{a_2}\ddot{\mathbf{a}}, \tag{2b}$$

where $\mathbf{a} = \{\mathbf{q}; \mathbf{v}_g/V_\infty\}$, by means of a rational approximation reduced to minimum states through a balanced truncation (Ref. 17). The DLM method considers potential flows, and it is based on panels defined on a flat lifting-surface plus the inclusion of a flat wake. It considers only small out-of-plane harmonic motions, and consequently it is not able to compute any aerodynamic derivative for in-plane motions or contributions of steady/unsteady drag forces. However, this approximation has a limited impact on tiltrotor unsteady aerodynamics, because the largest in-plane forces are generated by the aerodynamics of proprotor oscillations, included in rotor dynamics models.

Rotor aeroelastic models are obtained from CAMRAD/JA using data published by Acree in Ref. 18. Rotor dynamics are generally described by nonlinear differential equations, which can be linearized for a subset of trim configurations representative of the flight conditions of interest. Linear time invariant (LTI) models are computed using coefficient averaging to eliminate any periodicity whenever the rotors are not in axial flow conditions. A robust interpolation method is subsequently used in MASST to estimate rotor models for any intermediate trim point (Ref. 4). Rotor blade aerodynamic forces are calculated using lifting line theory and steady, two-dimensional airfoil characteristics, with corrections for unsteady and

three-dimensional flow effects (Ref. 19). C81 tables are provided by Acree in Ref. 18, in which lift, drag and pitching moment coefficients related to the XV-15 ATBs are tabulated versus angle of attack, covering the full $\pm 180^o$ range, and several Mach numbers ranging from 0 to 1. The momentum theory induced velocity model is also included; empirical corrections to account for non-ideal induced power losses and a linear variation of the induced velocity over the rotor disk due to non axial flow are defined in Ref. 18. Collective and cyclic modes have been considered for the three-bladed, gimballed, stiff-in-plane XV-15 rotors, respectively: two bending modes, one torsion mode and the two gimbal modes (longitudinal and lateral). According to Ref. 5, for proprotor stability analysis, only the fundamental modes below 1/rev are important. A higher bandwidth must be considered if an FCS that includes a load alleviation system is taken into account (see Refs. 20, 21). The two bending and the gimbal modes are selected to model the rotor cyclic flapping, lead-lag and rotor coning modes that lie in the frequency range of interest. The first torsion mode is related to the control chain compliance. This mode also provides the kinematic pitch-gimbal and pitch-bending couplings designed to reduce flapping and to keep the rotor flapping mode below 1/rev, reducing flap/lag instability in tiltrotors (Ref. 22). It must be remarked that the gimbal universal joint has been modeled as ideal homokinetic joint, neglecting the 2/rev components caused by rotor flapping (Ref. 23). Additionally, the three-state Pitt-Peters dynamic inflow model (Ref. 24) and the rotor speed degree of freedom, along with the six hub/pylon rigid modes required to connect the rotor to the airframe, have been taken into account. Thus, each rotor model contains 21 degrees of freedom. The XV-15 rotors are modeled with the composite Advanced Technology Blades. A database of linearized rotors has been generated in APMODE, at sea level standard (SLS) ISA* + 0°C conditions with limited power. For analysis, the rotor was trimmed to 480.8 rpm. The flight speed ranges from 140 to 400 knots, with flight speed steps of 20 knots. It must be noted that only the right-hand rotor has been modeled in CAMRAD/JA. The left-hand rotor is obtained in MASST, exploiting symmetry.

The dynamics of the engine-drive train system are modeled in MASST using simplified one-dimensional models consisting of a set of torsional springs and equivalent lumped inertias. The XV-15 engine-drive train model is derived from Ref. 19. In this work, a simplified model is proposed, consisting of a symmetric drive train system, shown in Fig. 3. Engines are approximated as lumped inertias while rotor nodes

*International Standard Atmosphere

are inertia-less, since rotor inertia is already included in the CAMRAD/JA rotor models. The connection between the engine drive-train system and the two rotors is made by the Craig-Bampton's component mode synthesis approach, through the rotor speed degree of freedom. The XV-15 reduced parameters I_E, K_E, K_M, K_I and the gear ratios, i.e. r_I and r_E, are derived from Ref. 18. The two gearboxes are joined by an interconnecting shaft. This system precludes the complete loss of power to either rotor due to a single engine failure, permits power transfer for transient conditions and provides rotational speed synchronization (Ref. 25).

The control surface deflections (flaps, flaperons, elevator, rudders) and the rotor pitch inputs (collective and longitudinal cyclic pitch) are actuated by hydro-mechanical servomechanisms, used for position control. Servo-actuators are represented in MASST by transfer functions that model the servo-valve and compliance dynamics (see Ref. 26, Chapter 9). The motion of a generic control surface, ϑ, is described as a function of the requested motion, ϑ_c, and of the generalized reaction moment applied by the dynamics of the control surface itself, m_c, namely:

$$\vartheta = H_c(s) \cdot \vartheta_c + H_m(s) \cdot m_c, \tag{3}$$

where $H_c(s)$ represents the servo-valve dynamics and $H_m(s)$ is the dynamic compliance. In the XV-15 MASST model, the servo-valve dynamics are described as a second order low-pass Butterworth filter, with a cut-off frequency of 15 Hz. The dynamic compliances of the airframe control surface servo-actuators have been estimated by considering a static stiffness of 200,000 lbf $\cdot$ in $\cdot$ rad^{-1}. These values have been selected by the authors to provide an adequate bandwidth for pilot's control and FCS authority, since no technical data concerning the XV-15 servo-actuators was found in literature. The dynamic compliance of the rotor pitch input servo-actuators have been neglected, since their contribution is included in the rotor control chain compliance.

Each substructure has been validated against the results provided by the corresponding reference papers, leading to a realistic tiltrotor model representative of an aircraft of the class of the XV-15. Further details on airframe natural frequencies and mode shapes, engine drive-train and rotor natural frequencies in a vacuum can be found in Ref. 11.

Flight Control System

The FCS is split into a Primary Flight Control System (PFCS) and an Automatic Flight Control System (AFCS). The PFCS contains the control laws necessary to maintain mission effectiveness, and include the pilot stick gearing functions and the "Beta" governor. The AFCS is designed to enhance flying qualities of the aircraft using feedback paths such as attitudes, rates and accelerations.

The XV-15 cockpit controls consist of a center stick, a collective-type power-lever and pedals for the pilot and copilot. A three-position switch on each power-lever controls the nacelle conversion angle. In APMODE, conventional airplane stick and rudder pedals are employed, whereas the collective stick/power-lever remains dedicated to providing power management. The rotor controls are phased out and control moments are generated with standard aerodynamic surfaces: the ailerons generate rolling moments, the elevator generates pitching moments, and the rudders generate yawing moments (Ref. 7). The PFCS manages the gear ratios between the control inceptors displacement and the control surfaces deflection, as a function of the flight speed and nacelle angle. The XV-15 scheduled gear ratios are provided by Ferguson in Ref. 27. The XV-15 used mechanical control linkages to generate the correct gear ratios, with the inclusion of two heavy mixing boxes placed in the fuselage and connected to nacelle tilting mechanism, as described in Ref. 7. In modern tiltrotors, mechanical transmission of control input is replaced by a fly-by-wire architecture.

Pilot selected rpm is maintained by a blade pitch or "Beta" governor. Traditionally, helicopters employ throttle governing where the pilot sets the collective pitch and the control system adjusts the engine power to maintain constant rotor speed. On the other hand, turboprops generally use Beta governing. If rotor speed decreases, the governor reduces blade pitch in order to match power available from the engine. For the specific tiltrotor case, a helicopter governing scheme would encounter critical working conditions in APMODE configuration (Ref. 25). Due to the higher inflow ratios the torque exhibits high load variations for small collective pitch fluctuations. As a consequence, small power-lever displacements by the pilot would cause unsustainable torque transients. For this reason, an airplane-like "Beta" governing scheme was chosen during the XV-15 development, which was also considered suitable for the subsequent V-22 and AW609. The XV-15 "Beta" governor control law, reported in Ref. 18, is characterized by a

proportional-integral controller that considers as input the error between the requested and the measured rotor rpm. The controller gains (see Tables 17–I and 17–II of Ref. 27) are scheduled according to the nacelle angle.

The AFCS includes a Stability and Control Augmentation System (SCAS) on each axis, namely roll SCAS (RSCAS), pitch SCAS (PSCAS) and yaw SCAS (YSCAS). This is due to the tiltrotor characteristic response, that is essentially uncoupled in all flight modes. The control strategy implemented on the XV-15 is a Rate Command Attitude Hold (RCAH, see Ref. 28): the pilot moves the stick or pedals and a rate response is expected on the airframe (rate command mode); on the other hand, when the pilot does not use the cockpit controls (i.e. HANDS OFF) the attitude hold mode acts in the feedback loop. The SCAS provides attitude retention in all flight modes and uses three-axes-rate gyro packages to sense pitch, roll, and yaw rates and two attitude gyros to sense pitch and roll attitudes. Two different SCAS architectures have been derived for the XV-15: the original one was designed by Bell for the *S/N 702* prototype; the second, developed by NASA's Ames Research Center, was installed on the *S/N 703* prototype. The second one has been implemented in the MASST model. A brief description of the XV-15 SCAS architecture is reported in the following section, based on Ref. 29. The interested reader is referred to that document for further details.

The block diagram for the PSCAS is shown in Fig. 4. The RSCAS has the same architecture. Starting from the bottom, the block diagram shows a feedforward loop control shaping to provide desired response (rate/stick deflection) over the maneuver entry spectrum with time constant T_{1P}. The total control input due to the pilot is the sum of his mechanical input and that through the SCAS due to the gain K_{1P}, designed to cancel the original time constant. A stabilization loop – known as disturbance rejection mode – is designed to attenuate extraneous responses and disturbances within its prescribed bandpass (thus the time constant T_{2P}). Within the passband, lagged rate feedback (K_{2P}) is used to provide attitude stiffness, and simple rate feedback (K_{7P}) provides additional damping for the "pseudo" short period mode generated by this configuration. The pilot's input to the stabilization loop represents the desired command rate, modeled as a first order system, characterized by the time constant T_{1P} and steady state response $K_{4P} = q/X_{LN}|_{ss}$. This input is used to compute the tracking error, thanks to the rate sensor signal. The resulting system response to the pilot then becomes a rate command, attitude hold system over the

maneuver entry spectrum. The K_{3P} provides simple augmentation of the M_q stability derivative, adding an equivalent pitch damping. Finally, an attitude-hold circuit is introduced. It is turned OFF or ON by a switch on the SCAS panel. The condition of "HOLD OFF" corresponds to the pilot interaction with cockpit controls (in fact, it can be also defined as "HANDS ON") and the attitude feedback is high-pass filtered, viceversa for the "HOLD ON" mode. The PSCAS effect on tiltrotor dynamics is shown in Fig. 5. The aircraft response is evaluated as a function of a deterministic gust in APMODE at 140 knots. When considering a long gust profile (350 feet, Fig. 5(a)) the rigid body dynamics are mainly excited. The configuration with SCAS ON reaches first the steady state configuration with lower pitch rate/attitude amplitudes. The short gust (30 feet, Fig. 5(b)) also excites the SWB dynamics. However, the SCAS is still able to reduce the output response amplitude with faster transients. The YSCAS has a simpler structure (see Fig. 6) since the XV-15 response is relatively benign in the yaw axis and therefore it does not require the degree of stabilization provided in pitch and roll.

Again, starting from the bottom of Fig. 6, a feedforward loop control shaping is shown while the feedback loop is used to improve the yaw damping. All SCAS gains and time constants are scheduled with the nacelle angle and provided by Ferguson in Ref. 27.

A modified version is finally proposed for the yaw control of the XV-15 in APMODE, using differential collective pitch to generate yaw moments. This solution has contributed substantial cost and weight savings for the AW609. However, it is speculated here that possible SC mechanisms may arise if the YSCAS interacts with the anti-symmetric wing modes through the differential collective pitch control. The gear ratio between the pedal displacements and the differential collective pitch angle has been estimated by comparing the yaw rate response of the tiltrotor in APMODE, at different flight speeds. It was specifically designed by the authors of this work to match the low-frequency response obtained with the two rudders. This gear ratio is smaller than the one used for rudder control and characterized by a linear behavior with reference to the flight speed. While the gear ratio for rudders control is 8.0 deg/in, according to Ref. 27, the one used for differential collective control is equal to: $5.8 \cdot 10^{-3} V_\infty - 3.7 \cdot 10^{-1}$ deg/in, with V_∞ in knots. It was verified by comparing the time response of the rigid tiltrotor aircraft at 200 knots due to a pedal doublet input, including the SCAS. Fig. 7 shows that the yaw response obtained with the two rudders and with the differential collective pitch are in good agreement.

Pilot's Biodynamics Feedthrough

Pilots exert forces on aircraft inceptors thanks to neuromuscular activation of limbs, driven by the visual and vestibular perception of aircraft attitude and the proprioceptive perception of limb positions. Detailed physics-based models of pilots can be developed using a multibody approach, as done in Refs. 30, 31; however, those models are nonlinear, difficult to calibrate and characterized by a large number of degrees of freedom. This is due to the fact that muscular activation depends on many factors: biometrics of the pilot, shape and dynamics of inceptors, pilot skills, attention, mental state, workload etc. (see Ref. 32). An easier approach is based on the description of the pilot response through linear-frequency domain transfer functions, often obtained by experimental measures or from experience. Using this approach, it is common to consider separate independent transfer functions to model the voluntary and the involuntary parts of the pilot (see Fig. 1), although, in principle, the pilot model should be represented as a unique dynamic system. Using this second approach, it is possible to concentrate the attention on the transfer function representing the mechanical impedance that exists between the seat and the inceptors, that is usually denoted as biodynamic feedthrough (BDFT) Ref. 33. The BDFT should be a multiple-input multiple-output transfer matrix to model the transmission of the seat acceleration along three orthogonal directions to the movement of inceptors. However, the majority of models of this kind available in the literature, supported by experimental measurements, consider only the BDFT that connects the acceleration in one direction with the movement of one single inceptor. In this work, it has been decided to exploit only transfer function models based on experimental measurements, and thus cross coupling effects have been neglected.

Consequently, the involuntary pilot response acting on the power-lever due to a vertical acceleration, and the longitudinal and lateral stick movements due respectively to fore-aft and lateral accelerations are considered here. Given the significant variability of experimental results for pilots, see Refs. 32 and 33, it is important to select the worst-case scenarios, i.e. pilot's BDFT models that can represent the most destabilizing cases. This may not always be easy to achieve and often makes it necessary to perform specific tests for the determination of BDFT on the vehicle under analysis.

On each control inceptor, the pilot model is defined by a BDFT transfer function (TF):

1) Mayo (Ref. 34) identified a simple model of the BDFT that describes the action of helicopter pilots on the collective inceptor when subjected to vertical vibrations. In that case, results were obtained from two sets of pilots, identified as ectomorphic (small and lean build) and mesomorphic (large bone structure and muscle build). In this work, the ectomorphic pilot model is taken into account due to the lowest stability margins obtained in Ref. 11.

2) The longitudinal axis pilot's BDFT is derived from Ref. 6. This work presents pilot-in-the-loop aeroservoelastic analyses of the V-22. The longitudinal pilot's biodynamics was characterized by shaking pilots in the cockpit with hands on the controls.

3) Models of Ref. 35 are used to represent the pilot's BDFT along the lateral axis. According to the worst case scenario obtained in Ref. 11, the BDFT derived for test pilot 2 has been selected in this work.

The Bode diagrams of the selected pilot's BDFT models are shown in Fig. 8. The corresponding expressions for TFs can be found in Ref. 11.

Overall Stability Analysis

The closed-loop Pilot Vehicle System (PVS) block scheme is arranged in Fig. 9 including the tiltrotor basic aircraft, the FCS and the pilot's BDFT.

The aircraft model is trimmed to level flight up to the engine maximum power, and then allowed to descend as necessary to achieve the desired flight speed. The trim condition with limited power (i.e. level flight up to maximum power and constant power thereafter) was found to be critical for the basic aircraft stability boundaries in Acree et al. (Ref. 15). It may be possible that the inclusion of the SCAS and pilot's BDFT modifies the whirl flutter behavior of the aircraft, introducing other flight conditions in the flight envelope that are more prone to flutter than maximum power conditions. However, it has been decided to analyze maximum power flight conditions to allow a direct comparison between aeroelastic and aeroservoelastic stability.

The rotor is trimmed to 480.8 rpm, at sea-level standard conditions. The flight speed ranges from 140 to 400 knots, with trim and stability calculated in 20-knot increments. The power limit of 1550 hp is used,

necessary to level flight up to 280 knots. Table 3 lists the trim parameters obtained. It must be noted that the very low frequency behavior of SCAS and pilot's BDFT models is washed out, so the presence of those two systems does not interfere with the aircraft trim.

Four operative conditions are investigated:

- SCAS OFF, namely the basic tiltrotor aircraft without the FCS and without the pilot's BDFT;
- SCAS ON (HOLD ON), with the FCS set to attitude hold mode, without the pilot's BDFT;
- SCAS ON (HOLD OFF), with the FCS set to rate command mode and the pilot's BDFT in feedback loop;
- SCAS ON (HOLD ON) for the modified XV-15 using differential collective pitch to generate yaw moments, with the FCS set to attitude hold mode, without the pilot's BDFT.

All stability analyses in MASST are performed using a continuation procedure (Ref. 36), making it possible to follow the evolution of only the desired subset of eigensolutions of the system for the different parameter values. The low frequency flight mechanics roots and the six wing elastic modes are tracked using continuation with reference to the flight speed. Eigenvalues are shown in the Argand plane. The evolution of the wing elastic modes is also depicted in $V_\infty - \zeta$ plots.

It must be remembered that the airframe unsteady aerodynamics, obtained by the DLM, is not able to compute the stability derivatives due to unsteady drag forces when computing the aerodynamic generalized forces due to in-plane displacements. Table 4 shows the XV-15 flight mechanics roots obtained in MASST at 200 knots compared with analogous results provided by Ferguson with the Generic Tilt-Rotor Simulation code (GTRS, see Ref. 37), a model created for real-time flight mechanics simulations. The XV-15 MASST model is not able to capture the spiral mode, while the complex and conjugate phugoid is approximated as a stable heave subsidence mode. These results were expected since the two roots are characterized by a drag and a side aerodynamic force component that are not correctly represented by the current unsteady potential flow for airframe aerodynamics. These limitations of the model are acceptable, since spiral and phugoid modes lie in the low frequency range of the rigid body flight mechanics, far below the airframe structural frequencies of interest for SC problems. Conversely, roll subsidence, short period

and dutch roll are present in the XV-15 MASST model and the values are close to the ones computed by GTRS.

Overall stability maps are shown in Fig. 10, while $V_\infty - \zeta$ plots are reported in Fig. 11. A modal structural damping of 1% is considered for each airframe mode.

The SCAS OFF model is characterized by two unstable roots. Figure 10(a) shows that SWC and AWB are the critical modes, as shown in Ref. 15. The SWC is shown to be critical at 297 knots while the AWB at 307 knots (see Fig. 11(a)). The SWT instead reaches the stability boundaries at 380 knots although the damping ratio increases shortly after.

The second configuration, SCAS ON (HOLD ON), shows SC problems due to FCS (see Fig. 10(b) and Fig. 11(b)). Although the AWB mode is highly damped and stable all over the flight envelope, when the FCS is included, spillover effects arise on the AWT mode that becomes unstable at 289 knots. Some screenshots of the corresponding flutter mode shape at 289 knots are shown in Fig. 12. The highest modal participation is due to the antisymmetric wing torsion, although the coupling with the chordwise wing bending is clearly visible. Both regressive lead-lag and gimbal modes are participating together with flaperon and rudder deflections driven by the RSCAS and the YSCAS. The gyros sense the roll and the yaw rates due to wing elastic deformation, causing a delayed flaperon activation. The phase shift between the flaperons' activation and the wing torsion that causes the whirl flutter aeroservoelastic instability can be observed in Fig. 12 and computed by the corresponding flutter eigenvector, leading to a result of approximately 110°. The sensitivity analysis reported in the next paragraph reveals that the problem is traced to the roll rate feedback gain in the RSCAS stabilization loop, which cancels the stability of the AWT mode, while the YSCAS has a smaller (and stabilizing) effect. In addition, a second flutter appears because the PSCAS modifies the dynamics of the short period mode, now characterized by an augmented damping ratio and frequency. This mode in turn couples with the lightly damped SWB mode that becomes critical at 354 knots. The SWB mode shape is now characterized by an elevator deflection due to the pitch rate stabilization loop, that causes the coupling of wing bending with the aircraft pitch motion. Conversely, the SWC mode is not modified by the FCS. It shows the same trend seen for the SCAS OFF model. Of course, the FCS is also acting on the low frequency flight mechanics roots that move towards the left part of the Argand plane.

The flutter margin is further reduced when the pilot's BDFT is included in the feedback loop, as shown in Fig. 10(c) and Fig. 11(c). A resonance between the pilot's biomechanics acting on the power-lever and the aircraft SWB is shown starting at the minimum flight speed. This phenomenon was analyzed and discussed in Ref. 11, where the source of instability was identified in the symmetric torque generated by the counter-rotating rotors after a throttle input through the power-lever. The instability is similar to a vertical bounce since the SWB magnifies the vertical accelerations and, in turn, through pilot's biomechanics, the power-lever input. Similarly, a SC phenomenon due to longitudinal pilot BDFT coupled with the SWC mode is observed. In this case, the pilot's involuntary input to fore/aft center stick is subjected to PSCAS control shaping to produce a pitch rate command. The corresponding pitch motion resulting from the elevator deflection excites the longitudinal aircraft dynamics, reducing the stability margins of the lightly damped SWC mode. The whirl flutter speed is reduced to 253 knots by including the BDFT. For antisymmetric modes, the RSCAS stabilitation loop reduces the stability of the AWT mode that becomes unstable at 285 knots, as happened in the previous case.

Finally, the modified version of the XV-15 with yaw control on rotors is characterized by a SC problem on the AWC mode. As expected, the YSCAS acts on the differential collective pitch to increase the yaw damping. However, it must be remembered that the thrust exhibits high load variations for small collective pitch angles, due to the higher inflow ratios in APMODE. The resulting antisymmetric thrust forces act on the two rotor hubs where the AWC modal participation is the largest. This configuration reduces the AWC damping ratio that leads to a flutter at 168 knots (see Fig. 10(d) and Fig. 11(d)), severely limiting the flight envelope unless appropriate filtering is used. Moreover, the AWT is also characterized by a reduced flutter speed that reaches the value of 229 knots. The SWC and the SWB become unstable at the same speeds already computed for the SCAS ON (HOLD ON) standard configuration. The inclusion of the pilot's BDFT further reduces these last two flutter speeds, through the same mechanisms already described.

Table 5 summarizes all the critical speeds (from the lowest to the highest) obtained for the basic and augmented aircraft configurations considered in this analysis, and also lists for each of them the corresponding mode shape that becomes unstable.

Sensitivity analysis

To verify if the SC phenomena presented in the previous section are the consequence of the limited aeroelastic stability of the thin-wing (15% t/c), it has been decided to perform the analyses also using the thick-wing (23% t/c), that does not show any flutter up to 400 knots. The MASST model has been modified according to the airframe thick-wing stick model proposed by Acree et al. in Ref. 15, even though that model was not fully correlated with the ground vibration test results of the XV-15 prototype. The critical speeds obtained for the basic and augmented thick-wing aircraft are listed in Table 6. The table shows that even this more stable configuration shows significant SC effects. In particular the SCAS ON (HOLD ON) configuration reveals an instability involving the AWC mode at 243 knots, below the corresponding flutter speed of the thin-wing. This flutter is characterized by a similar mechanism to the one already described for the thin-wing but it happens at a lower speed because the AWC mode contains a large participation of the wing torsion.

Structural coupling mechanisms have been further investigated through a sensitivity analysis to the SCAS gains and to pilot's BDFT static gains and time delays, with reference to the thin-wing configuration. All analyses are performed at 360 knots.

Figure 13 shows the airframe symmetric roots for different PSCAS gains. Gains have been modified by halving and doubling their nominal values. Starting from the disturbance rejection mode stabilization loop, the sensitivity to the lagged rate feedback gain K_{2P} shows a mild impact only on the SWB mode, slightly decreasing the damping ratio when doubling the gain. Conversely, the rate feedback gain K_{7P} shows a large damping sensitivity for all symmetric modes. The SWT and SWC damping ratios increase with the gain, while the opposite trend is shown for the SWB mode. Sensitivity to the pitch rate feedback gain is not presented, since the K_{3P} nominal value is null in APMODE, while the K_{5P} pitch attitude feedback gain shows almost the same trend of K_{2P}. So, in conclusion all PSCAS gains have a negative impact on the SWB stability, while K_{7P} has a stabilizing effect on SWC and SWT.

Sensitivity analyses to RSCAS gains are shown in Fig. 14. The roll rate feedback gains, K_{7R} and K_{3R}, mainly reduce the AWB and the AWT damping ratios revealing similar trends, although the highest variations are due to K_{7R}. The analysis shows how a sharp reduction of the roll rate feedback gains can

stabilize the AWT mode. However, the modification of K_{3R} changes the desired roll response, through the stability derivative L_p, while a reduction of K_{7R} reduces the authority of the stabilization loop.

Figure 15 shows the modification of the airframe antisymmetric modes due to K_{2Y} gain. It is interesting to notice that the yaw rate feedback gain improves the stability of the AWT and AWC modes when the yaw control moments are generated by the two rudders, while it slightly reduces the damping ratio of the AWB. A different trend is shown when using the differential collective pitch for yaw control. Doubling K_{2Y} all antisymmetric airframe modes decrease the damping ratios.

Pilot's BDFT has shown a large inter–subject (i.e., between different subjects) and intra–subject (i.e., on the same subject in different tests) variability (Ref. 38), so it is important to assess the sensitivity to gain and phase represented through time delays. Doubling the pilot's static gain magnifies the vertical bounce, which drastically reduces the SWB damping ratio, as shown in Fig. 16(a). Similarly, the stability boundaries of the SWC are further reduced when the longitudinal axis pilot's gain is increased. The introduction of a time delay modifies the SWT mode as well, decreasing the damping ratio as a result of the out-of-phase fore/aft stick displacements due to longitudinal pilot's BDFT, as shown in Fig. 16(b). Time delay on the pilot's biodynamics acting on the power-lever has a mild impact on the vertical bounce phenomenon.

Mitigating Solutions for Structural Couplings

The results obtained in this study point out that both the FCS and the pilot's BDFT decrease the stability margins of the tiltrotor aircraft. All the critical speeds are reduced when considering the closed loop PVS and many SC problems arise. Means of prevention are discussed in this section and implemented on the thin-wing XV-15 model.

The introduction of a low pass, second order, Butterworth filter on rate measures is initially investigated as a way to prevent the SC mechanisms. Fig. 17 shows the wing elastic roots at 400 knots computed for the SCAS ON (HOLD ON) configuration with different cutoff frequencies on the low pass Butterworth filter. With a 10 Hz cutoff frequency the AWC and the SWT are found to be unstable (the two eigenvalues were originally well damped). The AWT and the SWC roots move toward the right half of the Argand

Plane. The same trend is shown for the SWB mode, although in a less evident way. Only the AWB slightly increases the damping. The situation gets worse if the cutoff frequency is reduced to 5 Hz, except for the AWC mode that returns into the stable region. All the SC effects disappear if the cutoff frequency is further reduced to 1 Hz, returning to the standard aeroelastic instabilities shown by the aircraft without SCAS or pilot's BDFT. However, with a cutoff frequency of 1 Hz the FCS does not have adequate bandwidth to control the tiltrotor rigid body dynamics, losing its authority on flight mechanics roots. The phase delay, due to the low pass filter, reduces the phase margin and stability boundaries of the closed loop system. It must be noted that the phase delay may also increase the PIO tendency of the aircraft. An alternative solution must be considered, one that is able to filter the undesired frequencies on the FCS loop without altering the phase behavior.

The design of notch filters is considered in the following, as a second approach to fix the SC problems. Notch filters (NFs) can suppress the resonance peaks of undesired modes. The structure of a NF, characterized by a second-order TF, is reported in Ref. 39. Four parameters can be selected for the NF: 1) the notch frequency ω_{NF}, 2) the slope in gain μ at the notch frequency, 3) the quality factor Q, where the effects of NFs are significant and 4) the non-dimensional gain value μ_∞ for infinite frequency. The Bode diagram of the NF with the corresponding design parameters is shown in Fig. 18. To correctly design the NFs, the Loop Transfer Functions (LTFs, see Ref. 40) must be provided on each feedback path. The XV-15 critical paths are summarized in Table 7, considering the four operative conditions investigated. Additionally, the critical wing elastic modes have been detected on each path and a specific NF has been designed to reduce the spill-over effects, as shown in Fig. 19.

To give an example, NFs have been designed at the outset to stabilize the closed loop PVS up to 300 knots, even though the certification will require the flutter-free flight envelope to be extended 15% above the maximum dive speed, so in this case up to 322 knots. Fig. 19(a) shows for example the LTF on the roll rate. Including the NFs, the LTF crosses the 0 dB axis only once, restoring a stable closed loop PVS. However, it must be remarked that, to obtain a stable and robust system, the NFs must be designed to guarantee a gain margin of 6 dB and a minimum phase margin of 60 degrees, according to Ref. 5. Similarly, NFs must be designed for the pilot's critical paths (see for example Fig. 19(b)). Stability analyses are then repeated, including the NFs, and $V_\infty - \zeta$ plots are shown in Fig. 20. For the two configurations

investigated, the airframe roots are stable up to 300 knots. The results obtained here support the conclusion that the NFs are the best solution to suppress SC problems since the elastic modes are filtered out from the signal injected to the actuators and the phase loss is reduced to a minimum. However, it must be remembered that NFs must be designed to work for all possible aircraft configurations, taking into account changes due to flight conditions, gross weight, center of mass and pilot's BDFT variability. This implies that the NF design shall cover the full range of stores and fuel levels in the whole flight envelope, without forgetting the pilot's uncertainty. In fact, it is known that humans can adapt the dynamics of their limbs by adjusting their neuromuscular activation, depending on factors such as task goals, spatial position, and orientation of the limbs, etc. (see Ref. 38), and it is likely that these adaptations may have a significant influence on the resulting BDFT. Consequently, several NFs must be designed, scheduled for the different configurations. The design process could often be complex, requiring specific optimization routines.

Conclusions

A detailed aeroservoelastic model, representative of the Bell XV-15 tiltrotor aircraft has been used to study structural coupling problems due to flight control system and to the pilot's biodynamic feedthrough. Moreover, a modified version of the XV-15, using differential collective pitch for yaw control in airplane mode instead of conventional rudders, as used in some tiltrotors like Leonardo AW609, has been investigated to show additional structural coupling problems due to this different mechanism for directional control.

The analysis performed demonstrated that the introduction of the flight control system generates structural coupling effects that can lead to reduction of the whirl flutter speed, or of the creation of new flutter mechanisms. Structural couplings have been highlighted both in the thin-wing configuration (15% t/c), naturally more prone to whirl-flutter, but also in the thick-wing configuration (23% t/c).

It is found that the roll rate stabilization loop degrades the stability of the anti-symmetric wing torsion mode, through a coupling with a delayed response of the flaperons. In addition, the pitch rate stabilization loop modifies the dynamics of the short period mode, which then couples with the symmetric wing bending mode.

The inclusion of pilots' biodynamic feedthrough has a significant impact on the whirl flutter stability leading to further limitations for the flutter-free flight envelope. A vertical bounce phenomenon appears at low flight speed, which in some cases may become the limiting factor for stability in forward flight. Moreover, the involuntary pilot input to the fore/aft stick reduces the stability margins of the lightly damped symmetric wing chord mode.

By using differential rotor collective pitch to control the aircraft about the yaw axis additional structural coupling effects on the anti-symmetric wing chord mode are identified, since the differential thrust forces provided by the yaw damper act on the two rotor hubs where the modal participation is the largest. This layout leads to reduced stability boundaries that have to be weighted against the vertical tail load reduction and consequent structural weight saving given by this aircraft configuration.

Notch filters are typically used to suppress structural coupling problems, reducing the flight control system gain and the pilot's input at the elastic mode frequencies, without introducing unacceptable low-frequency phase delays. The design of notch filters must consider the pilot's transfer function variability to obtain a sufficient robustness.

The paper showed how all tiltrotor subsystems, including the flight control system or pilot's biodynamic feedthrough, could potentially contribute to high-speed proprotor instability, and that complex diverging interactions may easily rise. Consequently, designers should carefully take into account these aspects starting from the early stages of preliminary and conceptual design of a new aircraft, in order to avoid surprises during the certification process.

References

[1]Stiles, L. R., Mayo, J., Freisner, A. L., Landis, K. H., and Kothmann, B. D., ""Impossible to Resist": The Development of Rotorcraft Fly-By-Wire Technology," Proceedings of the American Helicopter Society 60th Annual Forum, June 2004.

[2]Becker, J., Caldwell, B., and Vaccaro, V., "The Interaction of Flight Control System and Aircraft Structure," RTO AVT Specialists' Meeting on Structural Aspects of Flexible Aircraft Control, October 1999.

[3]Caldwell, B. D., "The FCS-Structural Coupling problem and its Solution," Flight Mechanics Panel Symposium, May 1994.

[4]Masarati, P., Muscarello, V., Quaranta, G., Locatelli, A., Mangone, D., Riviello, L., and Viganò, L., "An Integrated Environment for Helicopter Aeroservoelastic Analysis: the Ground Resonance Case," Paper 177, Proceedings of the 37th European Rotorcraft Forum, September 2011.

[5]Parham, T., Jr. and Corso, L. M., "Aeroelastic and Aeroservoelastic Stability of the BA 609," Paper G3, Proceedings of the 25th European Rotorcraft Forum, September 1999.

[6]Parham, T., Jr., Popelka, D., Miller, D. G., and Froebel, A. T., "V-22 Pilot-in-the-loop Aeroelastic Stability Analysis," Proceedings of the American Helicopter Society 47th Annual Forum, May 1991.

[7]Maisel, M. D., Giulianetti, D. J., and Dugan, D. C., *The History of the XV-15 Tilt Rotor Research Aircraft: From Concept to Flight*, The NASA History Series, Washington, D.C., 2000.

[8]Pavel, M. D., Jump, M., Dang-Vu, B., Masarati, P., Gennaretti, M., Ionita, A., Zaichik, L., Smaili, H., Quaranta, G., Yilmaz, D., Jones, M., Serafini, J., and Malecki, J., "Adverse rotorcraft pilot couplings — Past, present and future challenges," *Progress in Aerospace Sciences*, Vol. 62, October 2013, pp. 1–51. doi: 10.1016/j.paerosci.2013.04.003

[9]Mitchell, D. G. and Klyde, D. H., "Identifying a Pilot-Induced Oscillation Signature: New Techniques Applied to Old Problems," *Journal of Guidance, Control, and Dynamics*, Vol. 31, (1), 2008, pp. 215–224.
doi: 10.2514/1.31470

[10]Dieterich, O., Götz, J., DangVu, B., Haverdings, H., Masarati, P., Pavel, M. D., Jump, M., and Gennaretti, M., "Adverse Rotorcraft-Pilot Coupling: Recent Research Activities in Europe," Proceedings of the 34th European Rotorcraft Forum, September 2008.

[11]Muscarello, V., Colombo, F., Quaranta, G., and Masarati, P., "Aeroelastic Rotorcraft-Pilot Couplings in Tiltrotor Aircraft," *Journal of Guidance, Control, and Dynamics*, Vol. 42, (3), March 2019, pp. 524–537.
doi: 10.2514/1.G003922

[12]Reed, W. H., "Propeller-rotor whirl flutter: A state-of-the-art review," *Journal of Sound and Vibration*,

Vol. 4, (3), 1966, pp. 526 – 544.

doi: 10.1016/0022-460X(66)90142-8

[13]Masarati, P., Muscarello, V., and Quaranta, G., "Linearized Aeroservoelastic Analysis of Rotary-Wing Aircraft," Paper 099, Proceedings of the 36th European Rotorcraft Forum, September 2010.

[14]Craig, R. R., Jr. and Bampton, M. C. C., "Coupling of Substructures for Dynamic Analysis," *AIAA Journal*, Vol. 6, (7), July 1968, pp. 1313–1319.

doi: 10.2514/3.4741

[15]Acree, C. W., Jr, Peyran, R. J., and Johnson, W., "Rotor Design for Whirl Flutter: An Examination of Options for Improving Tiltrotor Aeroelastic Stability Margins," Proceedings of the American Helicopter Society 55th Annual Forum, May 1999.

[16]Albano, E. and Rodden, W. P., "A Doublet-Lattice Method for Calculating Lift Distributions on Oscillating Surfaces in Subsonic Flows," *AIAA Journal*, Vol. 7, (2), February 1969, pp. 279–285.

doi: 10.2514/3.5086

[17]Roger, K. L., "Airplane Math Modeling Methods for Active Control Design," Paper 4, AGARD Structural Aspects of Active Controls, Paper 4, AGARD-CP-228, August 1977.

[18]Acree, C. W., "An Improved CAMRAD Model for Aeroelastic Stability Analysis of the XV-15 with Advanced Technology Blades," Technical Memorandum 4448, NASA Ames Research Center, Mountain View, CA, March 1993.

[19]Johnson, W., *CAMRAD/JA, A Comprehensive Analytical Model of Rotorcraft Aerodynamics and Dynamics, Johnson Aeronautics Version*, Johnson Aeronautics, Palo Alto, CA, 1988.

[20]King, D. W., Dabundo, C., Kisor, R. L., and Agnihotri, A., "V-22 Load Limiting Control Law Development," Proceedings of the American Helicopter Society 49th Annual Forum, 1993.

[21]Miller, D. G., Black, T. M., and Joglekar, M., "Tiltrotor Control Law Design for Rotor Loads Alleviation Using Modern Control Techniques," IEEE American Control Conference, June 1991.

[22]Gaffey, T. M., "The Effect of Positive Pitch-Flap Coupling (Negative δ_3) on Rotor Blade Motion Stability and Flapping," Proceedings of the American Helicopter Society 24th Annual Forum, May 1968.

[23]Bilger, J., Marr, R., and Zahedi, A., "Results of Structural Dynamic Testing of the XV-15 Tilt Rotor

Research Aircraft," *Journal of the American Helicopter Society*, Vol. 27, (2), 1982, pp. 58–65.
doi: 10.4050/JAHS.27.58

[24]Pitt, D. M. and Peters, D. A., "Theoretical Prediction of Dynamic-Inflow Derivatives," *Vertica*, Vol. 5, (1), 1981, pp. 21–34.

[25]Schaeffer, J., Alwang, R., and Joglekar, M., "V-22 Thrust Power Management Control Law Development," Proceedings of the American Helicopter Society 47th Annual Forum, May 1991.

[26]Merritt, H. E., *Hydraulic Control Systems*, John Wiley & Sons, New York, 1967.

[27]Ferguson, S. W., "A Mathematical Model for Real Time Flight Simulation of a Generic Tilt-Rotor Aircraft," Contractor Report 166536, NASA Ames Research Center, Mountain View, CA, September 1988.

[28]Anonymous, "Performance Specification, Handling Qualities Requirements for Military Rotorcraft," ADS 33-E-PRF, US Army AMCOM, Redstone, Alabama, 2000.

[29]Churchill, G. B. and Gerdes, R. M., "Advanced AFCS Developments on the XV-15 Tilt Rotor Research Aircraft," Contractor Report 85A32013, NASA Ames Research Center, Mountain View, CA, May 1984.

[30]Masarati, P., Quaranta, G., and Zanoni, A., "Dependence of helicopter pilots' biodynamic feedthrough on upper limbs' muscular activation patterns," *Proc. IMechE Part K: J. Multi-body Dynamics*, Vol. 227, (4), December 2013, pp. 344–362.
doi: 10.1177/1464419313490680

[31]Masarati, P. and Quaranta, G., "Coupled Bioaeroservoelastic Rotorcraft-Pilot Simulation," Proceedings of ASME IDETC/CIE, DETC2013-12035, August 2013.

[32]Zanoni, A., Zago, M., Paolini, R., Quaranta, G., Masarati, P., Galli, M., Maisano, G., Ragazzi, A., Frigerio, L., and Murawa, M., "Flight Simulator Testing to Enhance Comprehension and Modeling of Rotorcraft Pilot Couplings," Proceedings of the American Helicopter Society 75th Annual Forum, 2019.

[33]Quaranta, G., Masarati, P., and Venrooij, J., "Impact of pilots' biodynamic feedthrough on rotorcraft by robust stability," *Journal of Sound and Vibration*, Vol. 332, (20), September 2013, pp. 4948–4962.
doi: 10.1016/j.jsv.2013.04.020

[34]Mayo, J. R., "The Involuntary Participation of a Human Pilot in a Helicopter Collective Control Loop," Paper 81, Proceedings of the 15th European Rotorcraft Forum, September 1989.

[35]Muscarello, V., Quaranta, G., Masarati, P., Lu, L., Jones, M., and Jump, M., "Prediction and Simulator Verification of Roll/Lateral Adverse Aeroservoelastic Rotorcraft-Pilot Couplings," *Journal of Guidance, Control, and Dynamics*, Vol. 39, (1), 2016, pp. 42–60.

doi: 10.2514/1.G001121

[36]Cardani, C. and Mantegazza, P., "Continuation and Direct Solution of the Flutter Equation," *Computers & Structures*, Vol. 8, (2), 1976, pp. 185–192.

doi: 10.1016/0045-7949(78)90021-4

[37]Ferguson, S. W., "Development and Validation of a Simulation for a Generic Tilt-Rotor Aircraft," Contractor Report 166537, NASA Ames Research Center, Mountain View, CA, April 1989.

[38]Venrooij, J., Abbink, D. A., Mulder, M., van Paassen, M. M., and Mulder, M., "Biodynamic feedthrough is task dependent," 2010 IEEE International Conference on Systems Man and Cybernetics (SMC), October 2010.

doi: 10.1109/ICSMC.2010.5641915

[39]Muscarello, V. and Quaranta, G., "Wing-Pilot Vertical Bounce in Tiltrotors," *Journal of Guidance, Control, and Dynamics*, Vol. 41, (8), August 2018, pp. 1731–1743.

doi: 10.2514/1.G002960

[40]Skogestad, S. and Postlethwaite, I., *Multivariable Feedback Control*, John Wiley & Sons, Chichester, 2005.

List of Figures

List of Tables

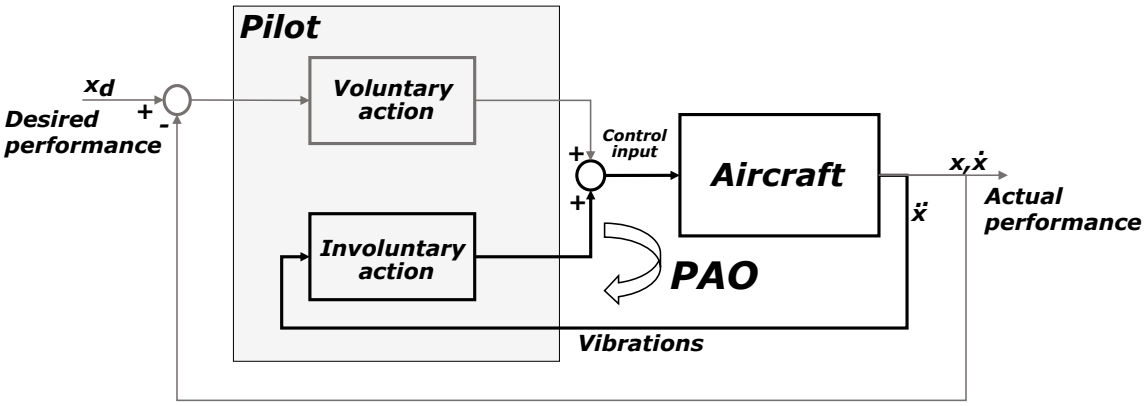

Fig. 1 Pilot-vehicle system with identification of voluntary and involuntary pilot feedback loops.

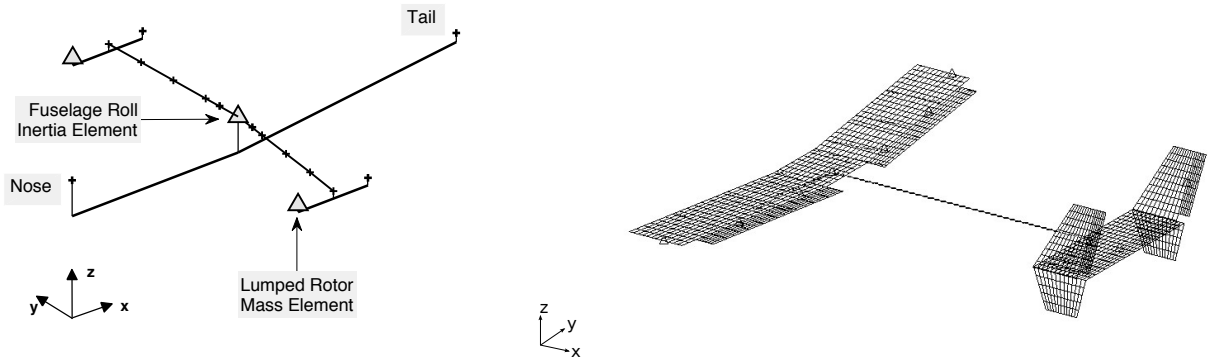

(a) Finite element stick model. (b) DLM: aerodynamic panels.

Fig. 2 Bell XV-15 airframe model.

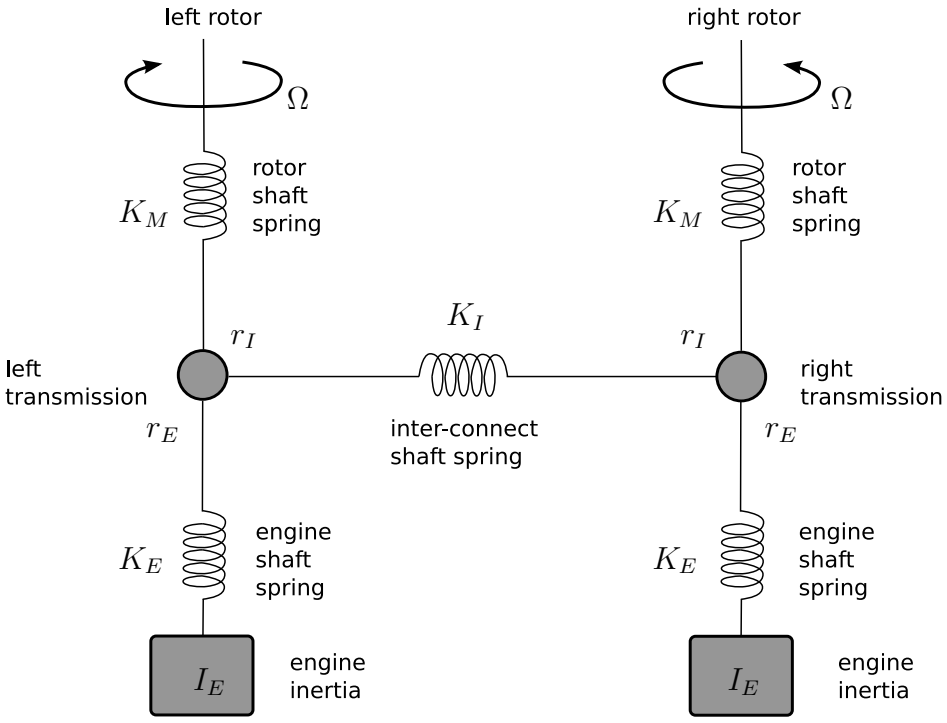

Fig. 3 Symmetric Engine - Drive Train model.

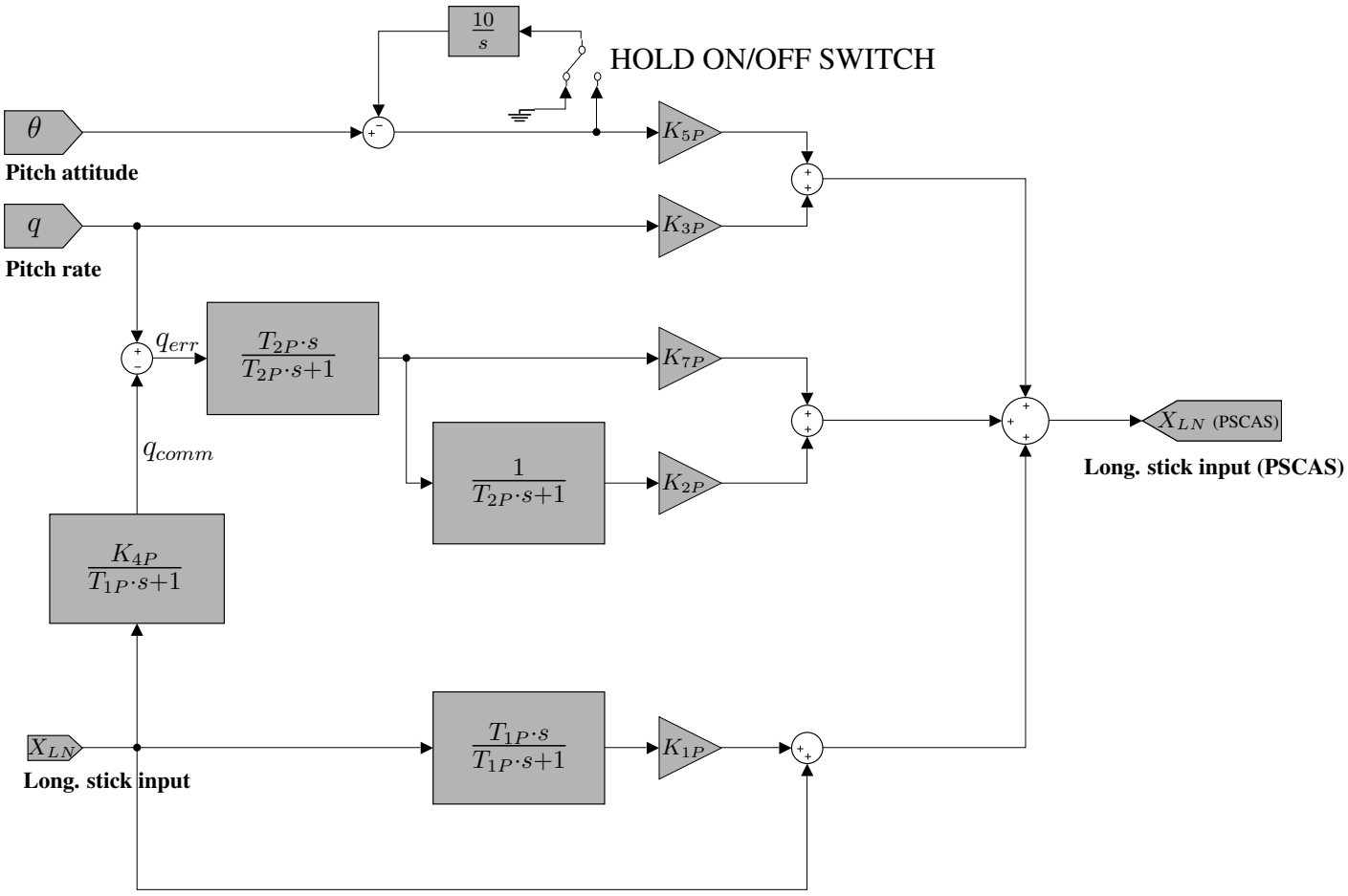

Fig. 4 PSCAS: simulink block.

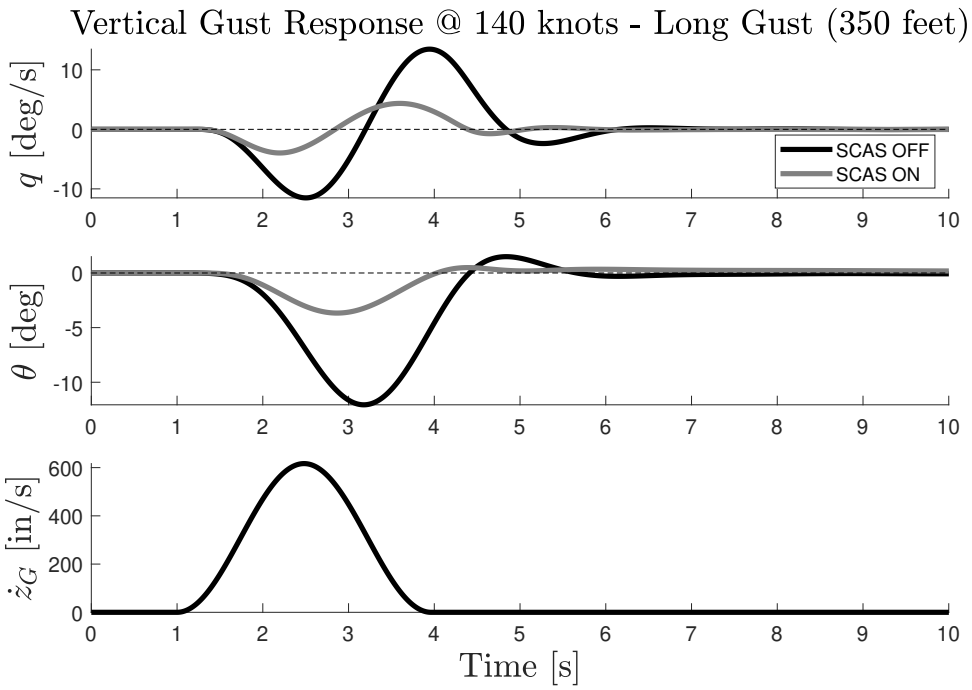

(a) Long gust (350 feet).

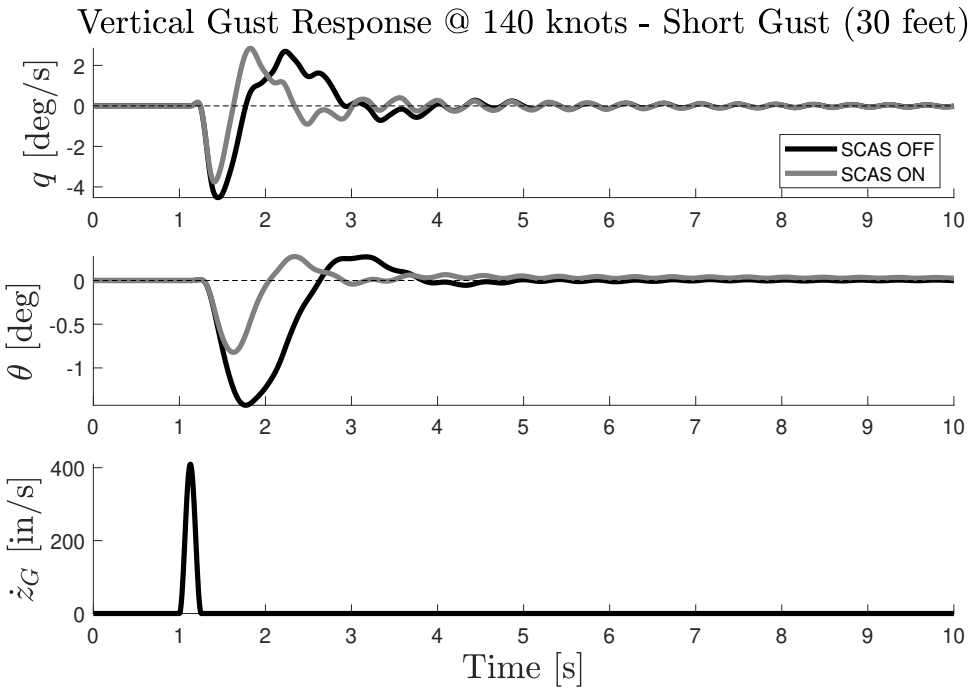

(b) Short gust (30 ft).

Fig. 5 Vertical gust response at 140 knots (APMODE), with/without SCAS (HOLD ON).

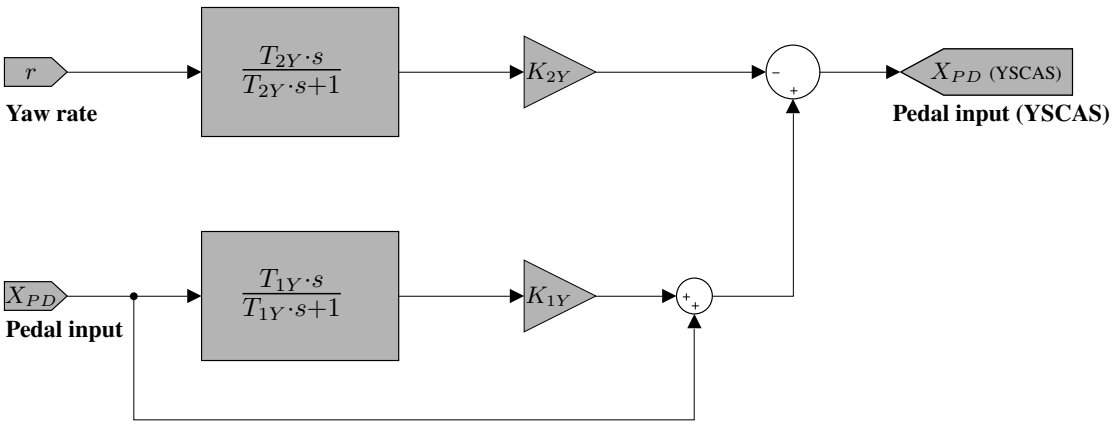

Fig. 6 YSCAS: simulink block.

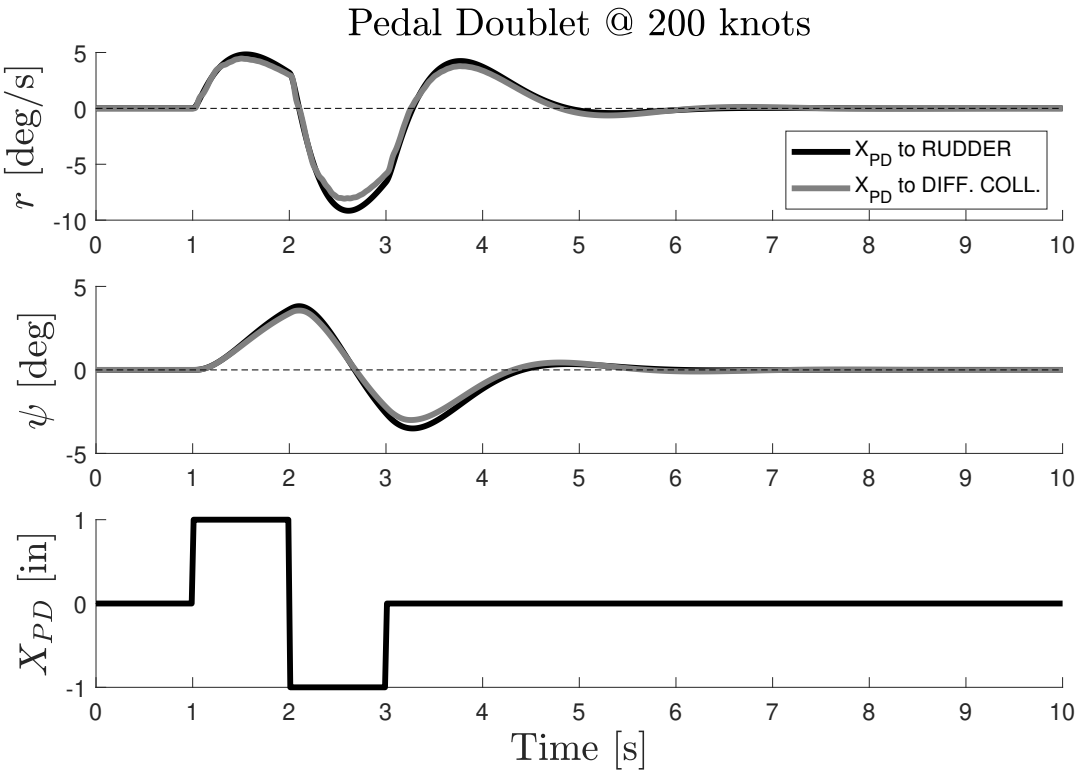

Fig. 7 Yaw response to pedal doublet at 200 knots (APMODE, rigid airframe), SCAS ON, obtained by rudder deflection – differential collective pitch.

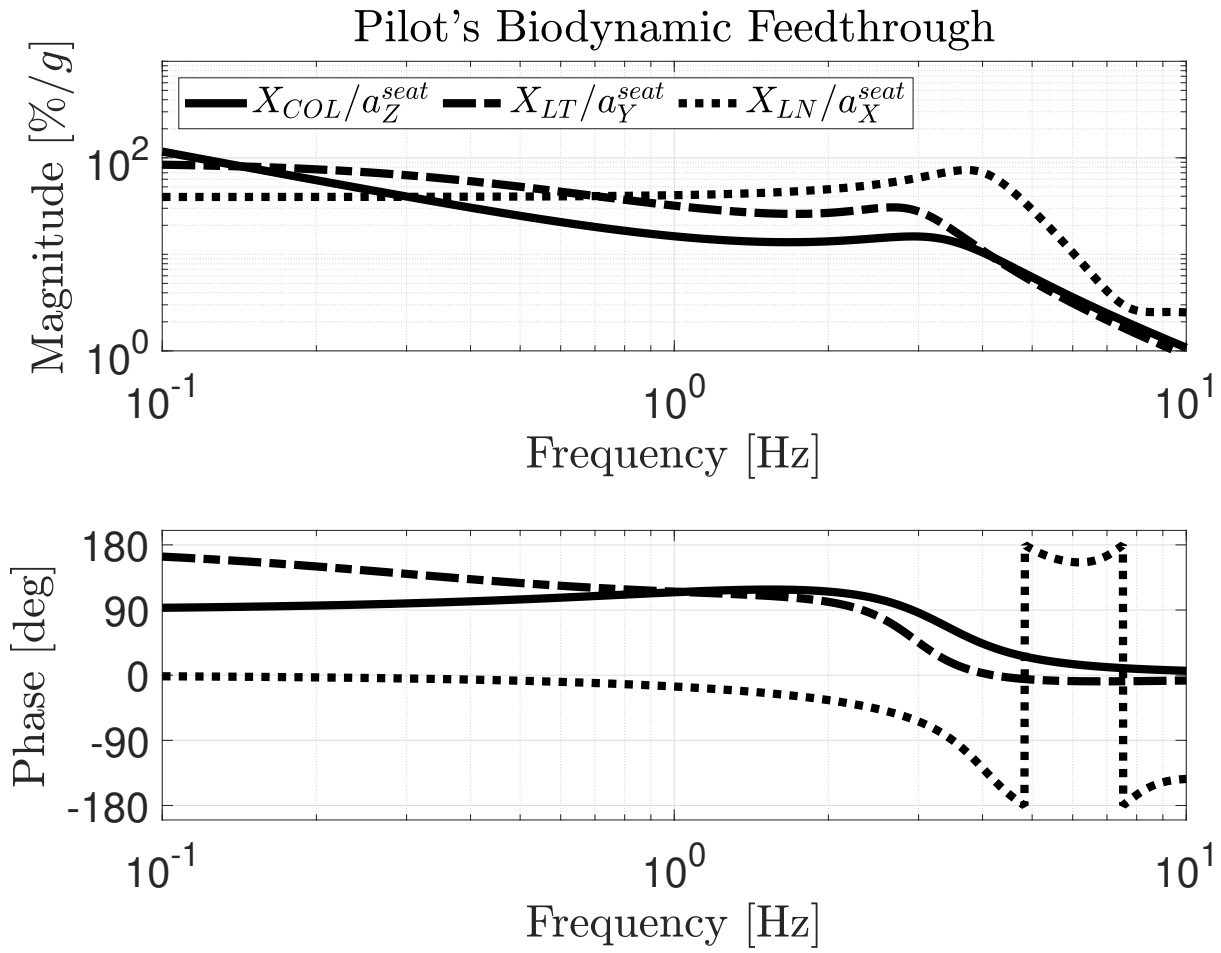

Fig. 8 Bode diagrams of the pilot's BDFT transfer functions acting on the power-lever, lateral and longitudinal control stick when subject to vertical, lateral and fore/aft seat accelerations.

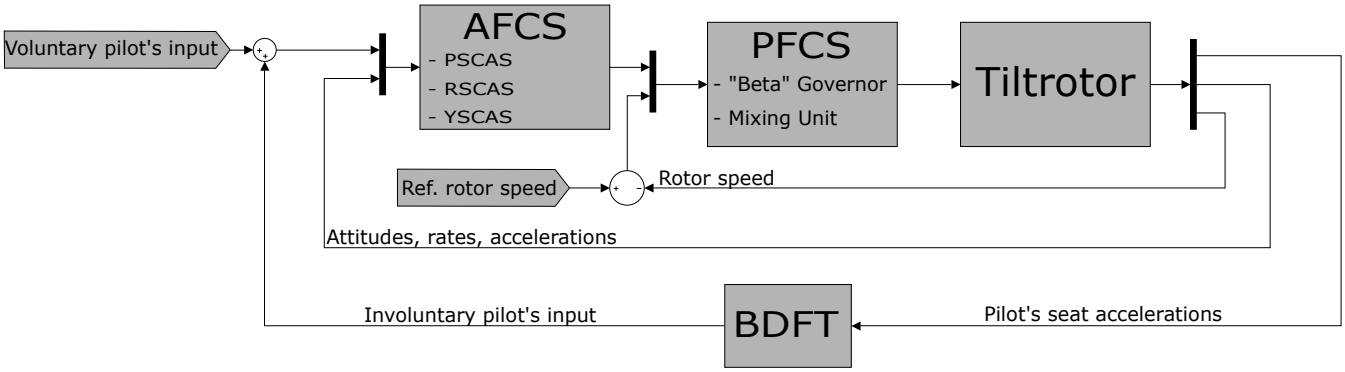

Fig. 9 Flow block diagram of the PVS.

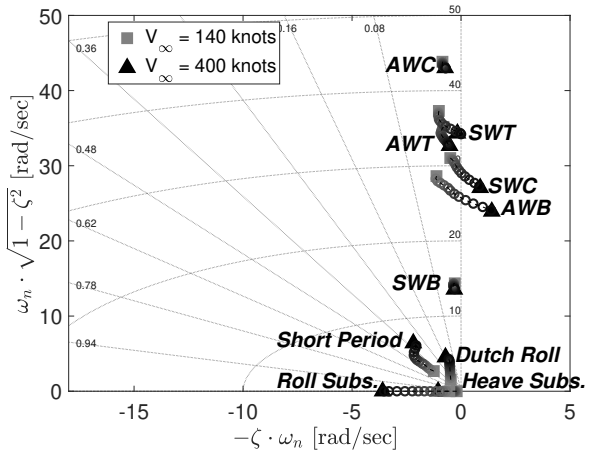

(a) SCAS OFF.

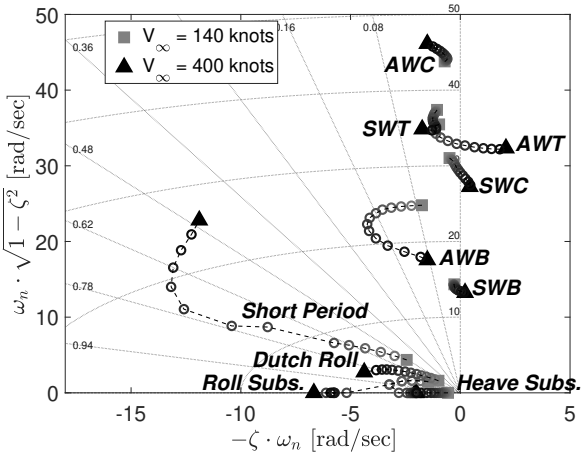

(b) SCAS ON (HOLD ON).

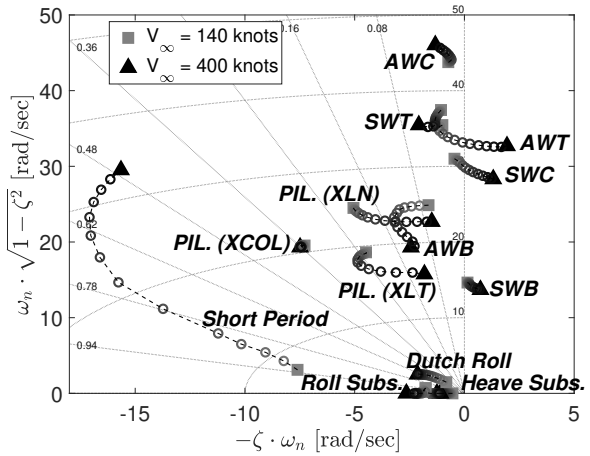

(c) SCAS ON (HOLD OFF) with pilot's BDFT.

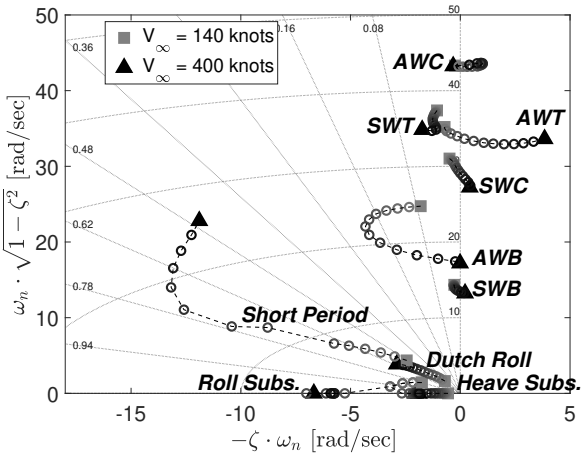

(d) SCAS ON (HOLD ON) with differential collective control.

Fig. 10 Overall stability maps.

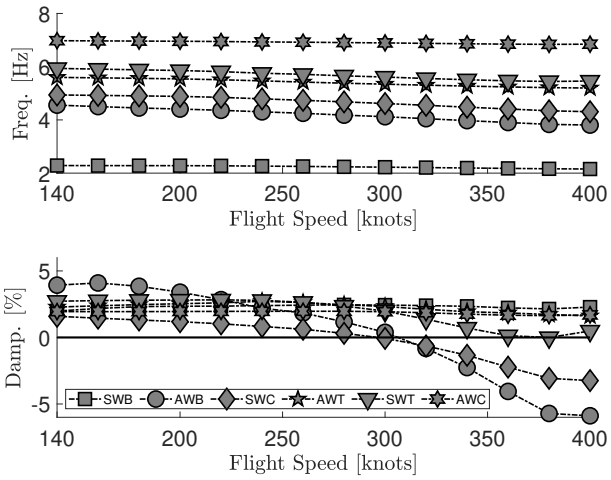

(a) SCAS OFF.

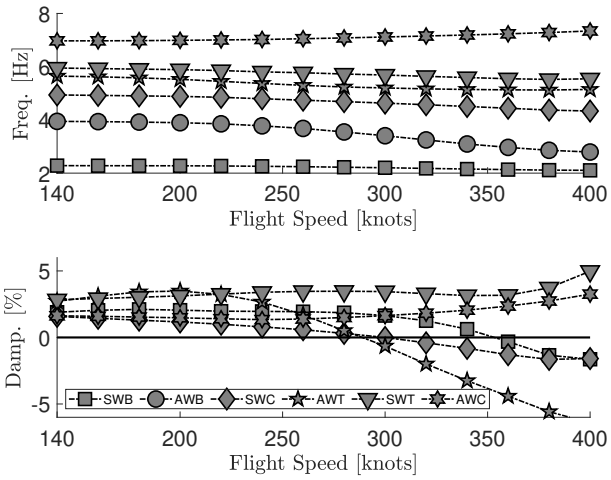

(b) SCAS ON (HOLD ON).

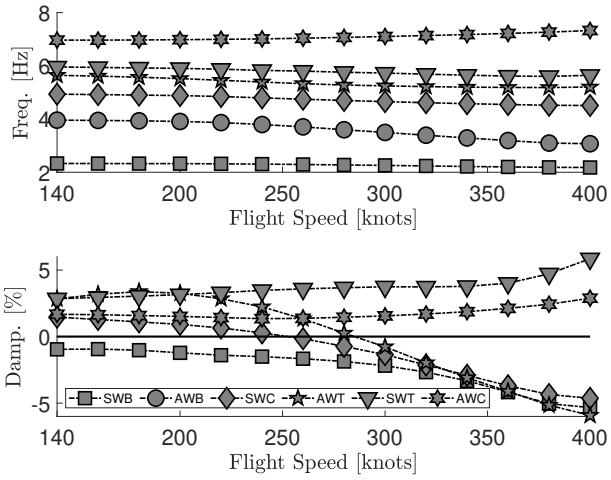

(c) SCAS ON (HOLD OFF) with pilot's BDFT.

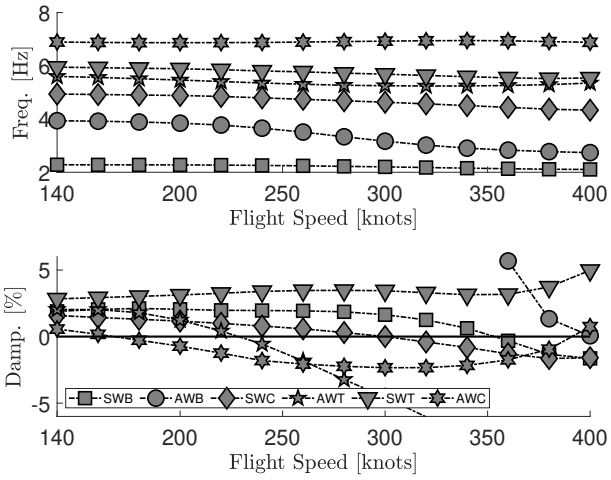

(d) SCAS ON (HOLD ON) with differential collective control.

Fig. 11 Frequency - damping ratio w.r.t. flight speed: wing elastic roots.

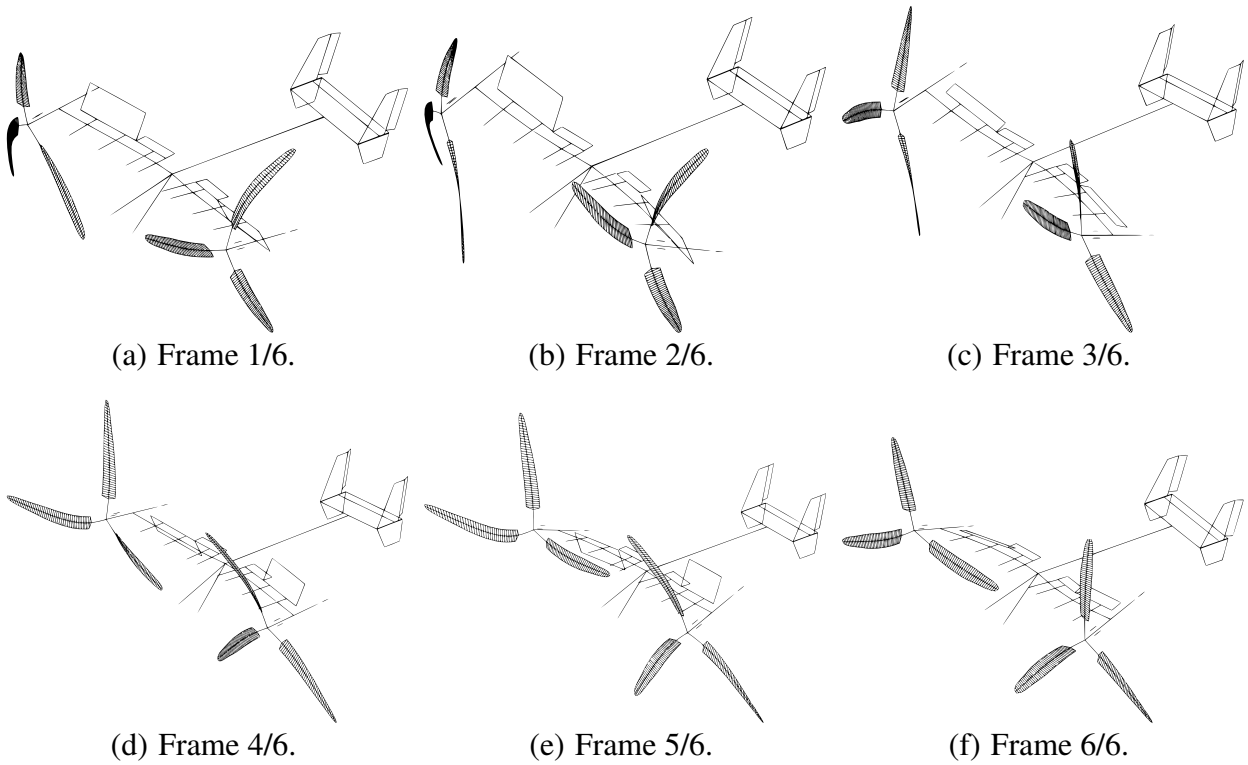

(a) Frame 1/6. (b) Frame 2/6. (c) Frame 3/6.

(d) Frame 4/6. (e) Frame 5/6. (f) Frame 6/6.

Fig. 12 Screenshots of AWT flutter mode shape at 289 knots - SCAS ON (HOLD ON) - equally spaced along the sinusoidal cycle, with rotor displacements and rotations visualized in the non-rotating reference frame.

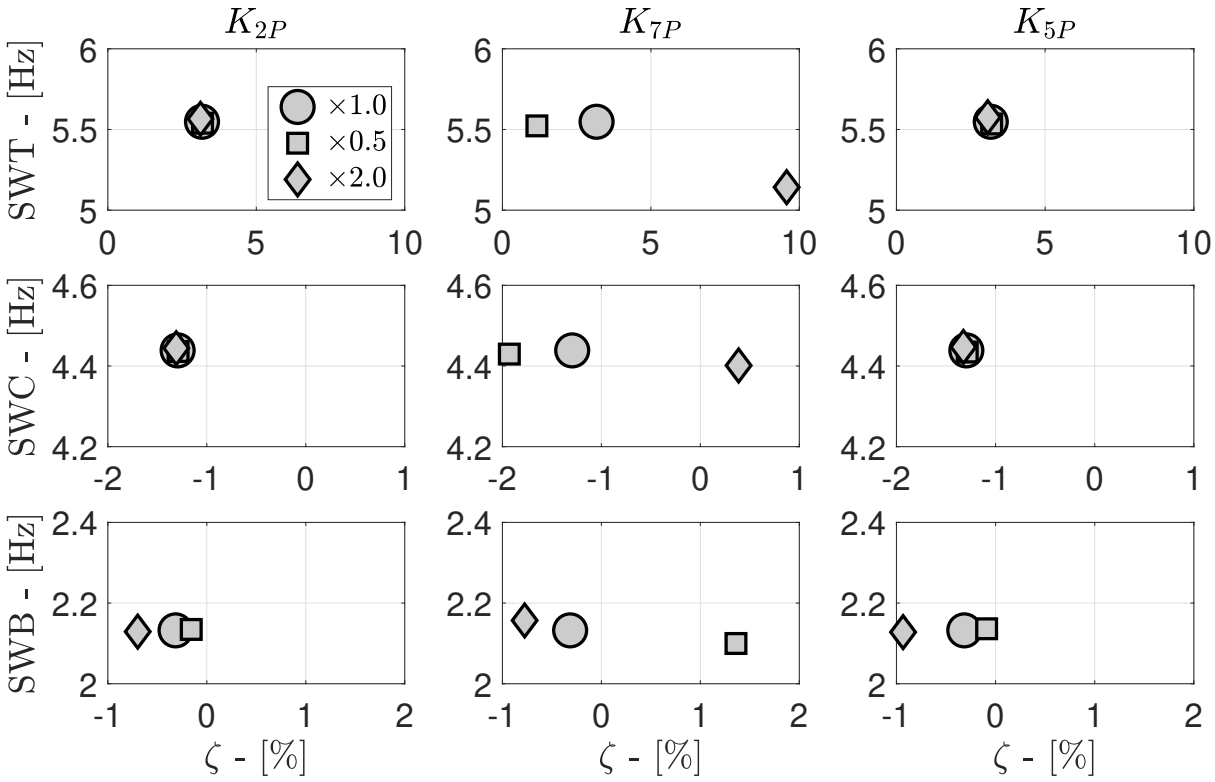

Fig. 13 Sensitivity analysis to PSCAS gains at 360 knots - SCAS ON (HOLD ON).

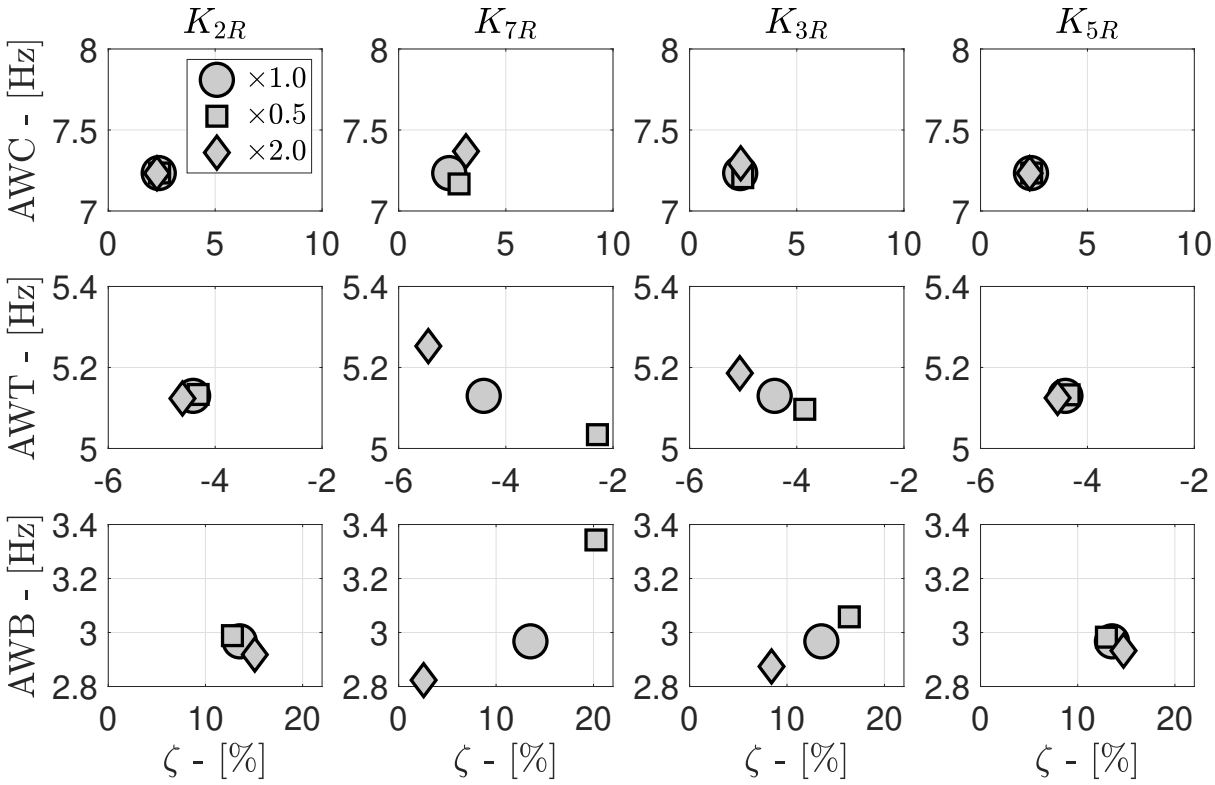

Fig. 14 Sensitivity analysis to RSCAS gains at 360 knots - SCAS ON (HOLD ON).

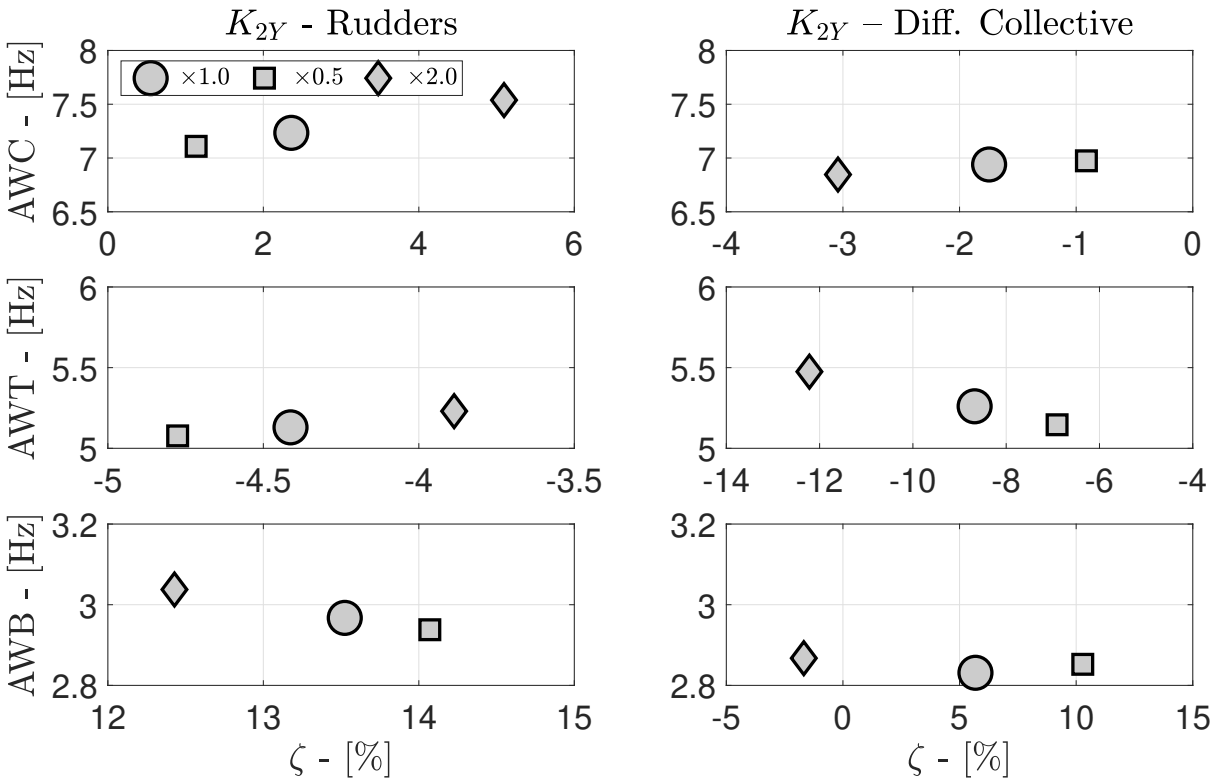

Fig. 15 Sensitivity analysis to YSCAS gains at 360 knots - SCAS ON (HOLD ON).

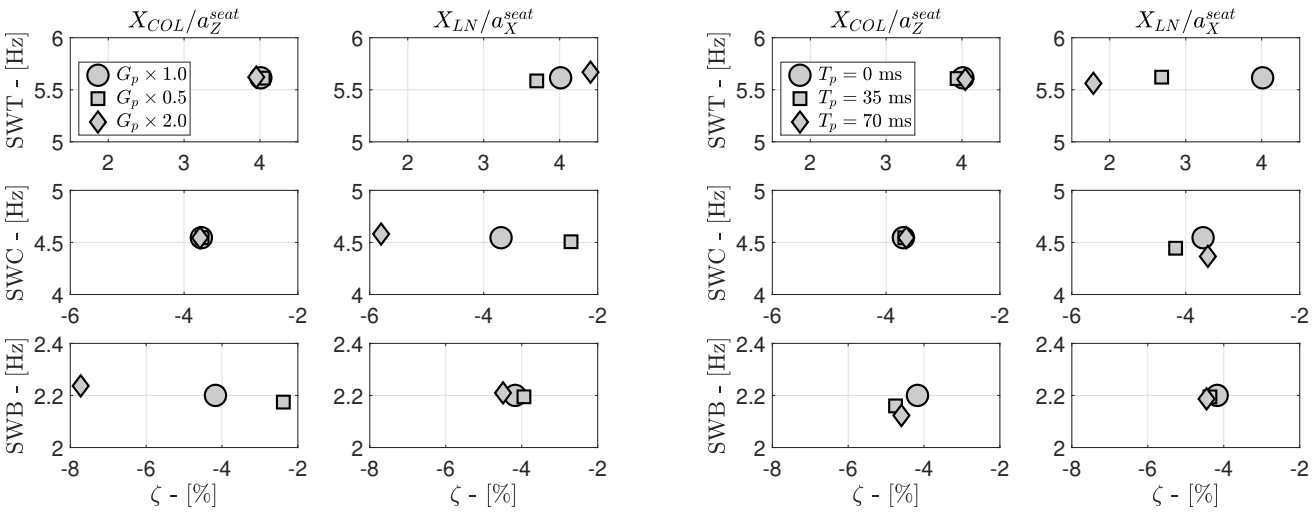

(a) Gain. (b) Time delay.

Fig. 16 Sensitivity analysis to pilot's BDFT gain and time delay at 360 knots - SCAS ON (HOLD OFF).

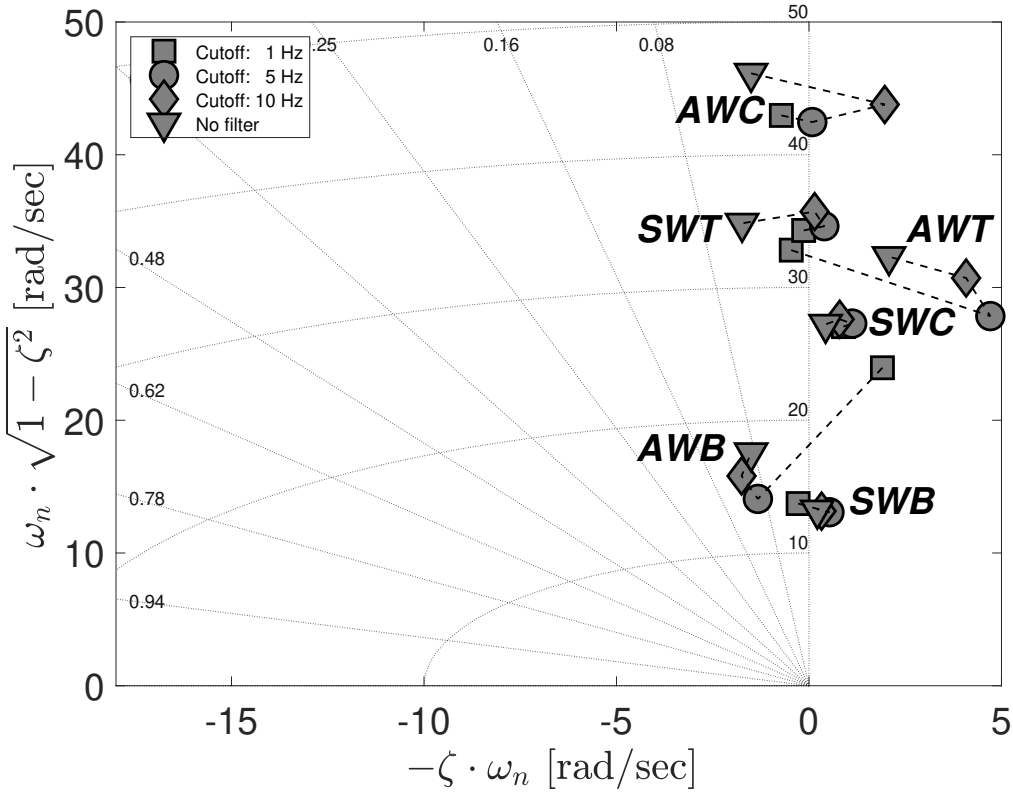

Fig. 17 Stability map at 400 knots, SCAS ON (HOLD ON). Effect of a second-order low-pass Butterworth filter (on rate measures) with different cutoff frequencies on wing elastic roots.

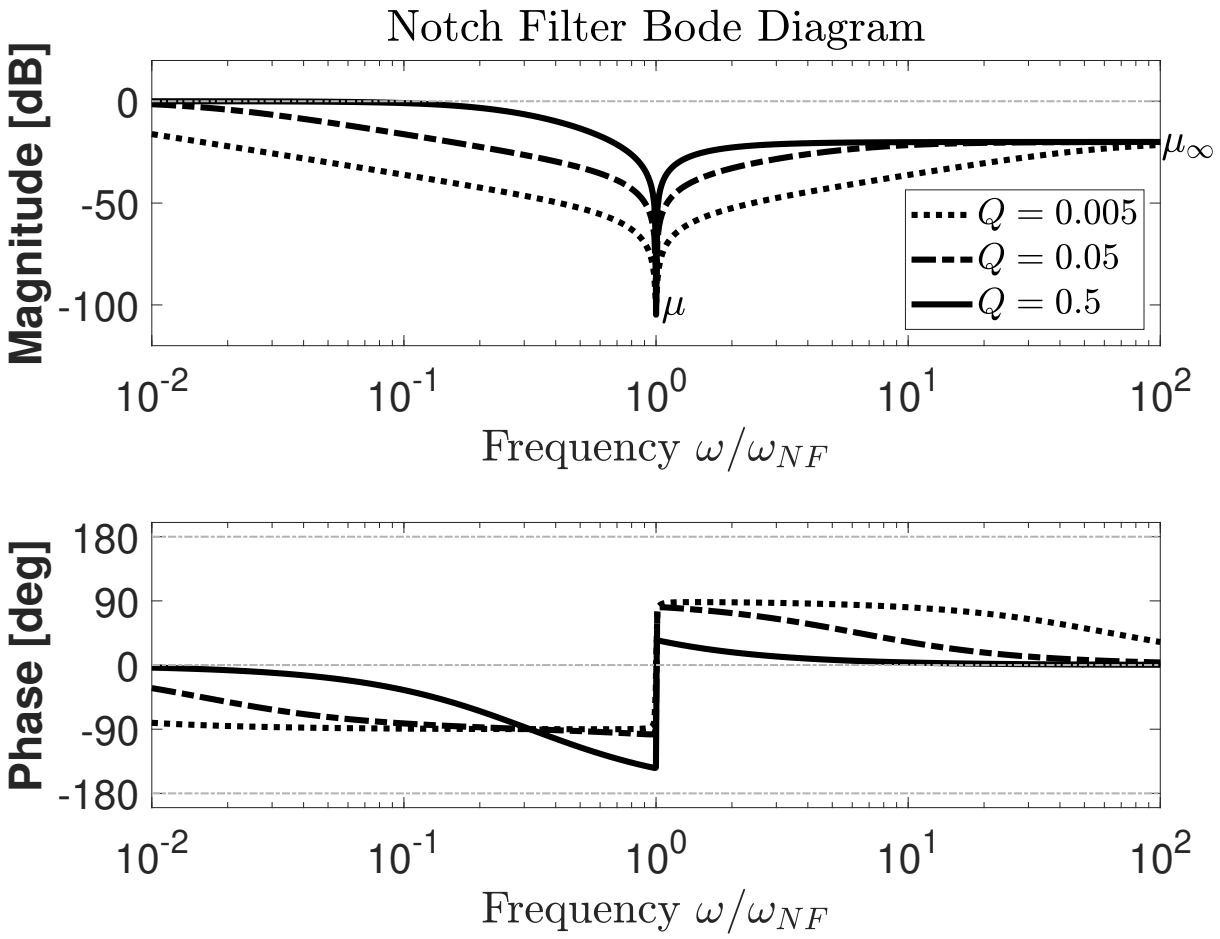

Fig. 18 Bode diagram of the notch filter.

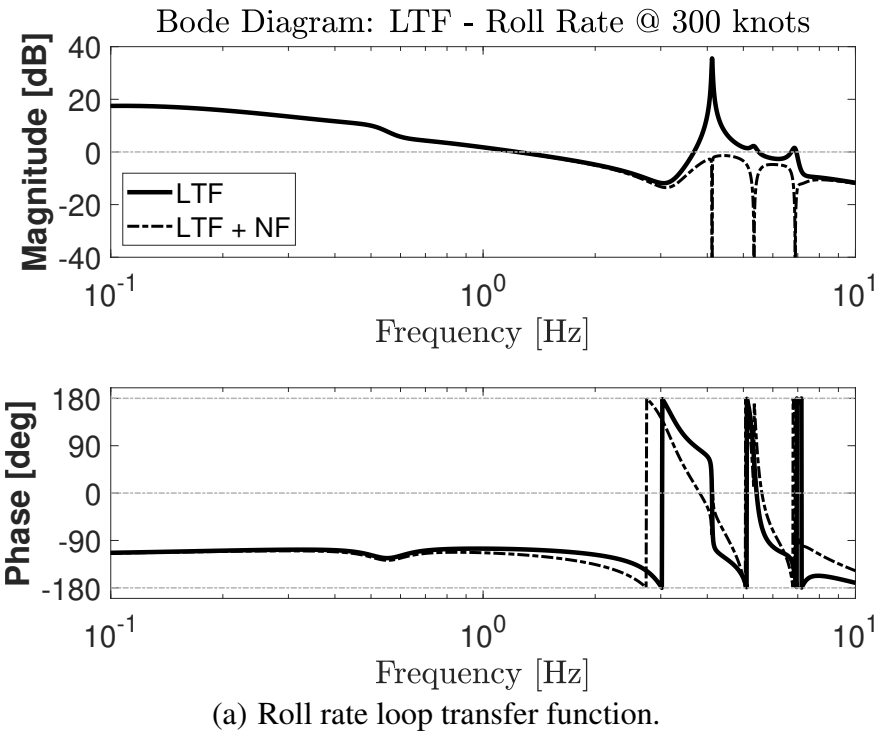

(a) Roll rate loop transfer function.

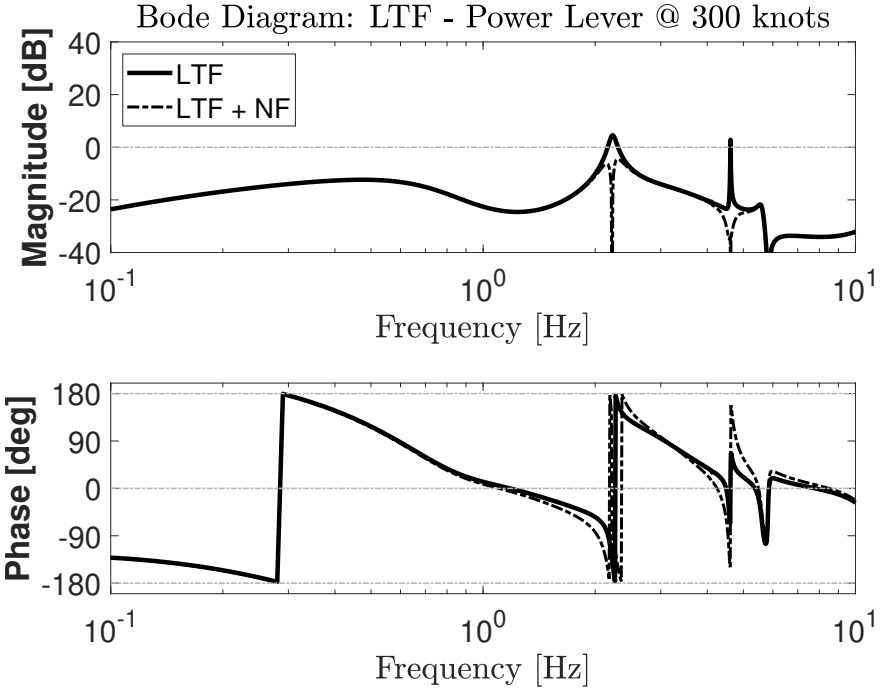

(b) Power-lever loop transfer function.

Fig. 19 Bode diagrams of the loop transfer functions with/without notch filters at 300 knots.

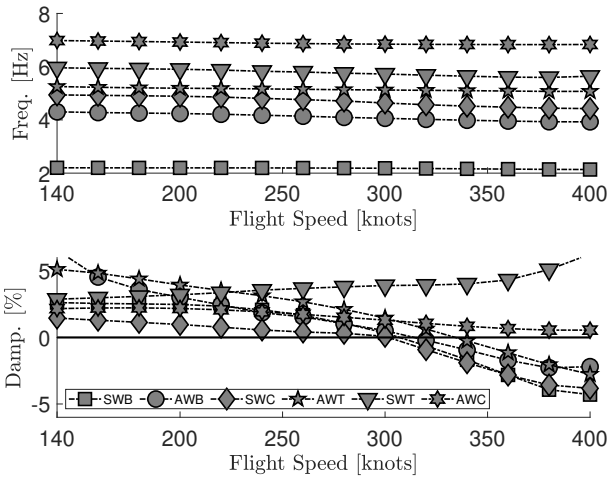

(a) SCAS ON (HOLD OFF) with pilot's BDFT.

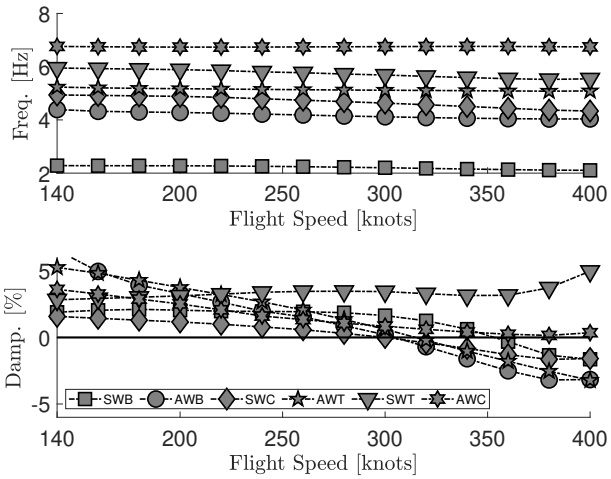

(b) SCAS ON (HOLD ON) with differential collective control.

Fig. 20 Notch filters effect. Frequency - damping ratio w.r.t. flight speed: wing elastic roots.

Table 1. XV-15 general characteristics.

Characteristic	**Symbol**	**XV-15 (ATBs)**	**Units**
Gross takeoff weight	W_{TO}	13,000	lb
Max. engine(s) power	P_{max}	2×1,550	hp
Max. flight speed	V_{max}	280	kt
Wing span	b	32.17	ft
Wing area	S	181.0	ft^2
Rotor radius	R	12.50	ft
Rotor solidity	σ	0.103	n.d.
Rotor Lock number	γ	3.768	n.d.
Rotor rotational speed	Ω	589*	rpm

*Reduced to 517 rpm in airplane mode.

Table 2. XV-15 airframe natural frequencies (APMODE).

Mode	**Frequency, Hz**	
	Thick-wing (23% t/c)	Thin-wing (15% t/c)
SWB	3.20	2.38
AWB	6.09	4.48
SWC	6.15	5.07
AWT	7.48	5.61
SWT	8.47	6.09
AWC	8.75	7.03

Table 3. XV-15 trim parameters in APMODE, SLS ISA + 0°C.

V_∞	δ_E^T	θ^T	τ^T	ϑ_0^T	ϑ_{1S}^T	β_0^T	β_{1C}^T	β_{1S}^T	T^T	P^T
kt	deg	deg	deg	deg	deg	deg	deg	deg	lb	hp
140	-1.27	6.84	0.00	29.43	-0.27	-0.07	0.17	-0.18	689	401
160	0.27	4.46	0.00	32.75	0.06	0.07	0.57	-0.03	696	467
180	1.25	2.82	0.00	35.82	0.26	0.18	0.99	0.13	744	554
200	1.91	1.65	0.00	38.67	0.40	0.28	1.42	0.31	823	661
220	2.36	0.79	0.00	41.31	0.50	0.37	1.87	0.51	926	791
240	2.61	0.17	0.00	43.73	0.55	0.43	2.38	0.78	1052	953
260	2.79	-0.31	0.00	45.96	0.59	0.48	2.91	1.06	1198	1148
280	2.91	-0.68	0.00	48.01	0.62	0.52	3.41	1.34	1360	1383
300	3.04	-1.97	-1.00	49.83	0.64	0.51	3.90	1.62	1426	1550
320	3.21	-4.97	-3.74	51.41	0.68	0.42	4.34	1.87	1310	1550
340	3.35	-8.05	-6.60	52.89	0.71	0.32	4.65	2.05	1196	1550
360	3.48	-11.37	-9.74	54.33	0.73	0.19	4.78	2.11	1070	1550
380	3.60	-15.10	-13.31	55.76	0.76	0.04	4.60	1.97	913	1550
400	3.73	-19.70	-17.77	57.26	0.79	-0.15	4.06	1.59	681	1550

Table 4. Flight mechanics roots at 200 knots (APMODE), basic aircraft – comparison between GTRS and MASST.

Mode	**GTRS** Eigen., rad/s	**MASST** Eigen., rad/s
Spiral	-0.1201	–
Phugoid	-0.2103± j0.1583	-0.2729*
Roll Subs.	-1.0648	-0.9437
Short Period	-2.0009± j3.2785	-1.6166± j3.3898
Dutch Roll	-0.5001± j1.7704	-0.4985± j2.2899

*Heave subsidence.

Table 5. XV-15 overall stability analysis: critical speeds.

SCAS OFF			SCAS ON (HOLD ON)			SCAS ON (HOLD OFF) - PIL. BDFT			SCAS ON (HOLD ON) - DIFF. COLL.		
V_{CR} knots	Mode	Fr. Hz	V_{CR} knots	Mode	Fr. Hz	V_{CR} knots	Mode	Fr. Hz	V_{CR} knots	Mode	Fr. Hz
297	SWC	4.63	289	AWT	5.22	140	SWB	2.28	168	AWC	6.87
307	AWB	4.09	300	SWC	4.63	253	SWC	4.76	229	AWT	5.38
–	–	–	354	SWB	2.14	285	AWT	5.27	300	SWC	4.63
–	–	–	–	–	–	–	–	–	354	SWB	2.14

Table 6. XV-15 thick-wing (23% t/c) overall stability analysis: critical speeds.

SCAS OFF			SCAS ON (HOLD ON)			SCAS ON (HOLD OFF) - PIL. BDFT			SCAS ON (HOLD ON) - DIFF. COLL.		
V_{CR} knots	Mode	Fr. Hz	V_{CR} knots	Mode	Fr. Hz	V_{CR} knots	Mode	Fr. Hz	V_{CR} knots	Mode	Fr. Hz
–	–	–	243	AWC	8.34	140	SWB	3.15	192	AWC	8.30
–	–	–	–	–	–	243	AWC	8.34	260	AWT	7.04
–	–	–	–	–	–	365	SWC	5.71	–	–	–

Table 7. XV-15 structural couplings summary.

Source	Critical path/s	Critical mode/s
Pilot's BDFT on vert. axis	Power-Lever	SWB
Pilot's BDFT on long. axis	Fore/aft stick	SWC
PSCAS	Pitch rate	SWB, Short Period
RSCAS	Roll rate	AWT, AWC*
YSCAS (RUDDERS)	Yaw rate	AWT
YSCAS (DIFF. COLL.)	Yaw rate	AWT, AWC

*Only for the modified XV-15 with differential collective pitch control.